Natural convection heat transfer from a vertical single cylinder with helical wire spacer in liquid sodium

Hata, Koichi

Liu, Qiusheng

Nakajima, Takashi

(Citation)
Nuclear Engineering and Design,341:73-90

(Issue Date)
2019-01

(Resource Type)
journal article

(Version)
Accepted Manuscript

Natural convection heat transfer from a vertical single cylinder with helical wire spacer in liquid sodium

Koichi Hata

Graduate School of Maritime Sciences, Kobe Univ.

5-1-1, Fukae-minami, Kobe, Hyogo 658-0022, Japan

Qiusheng Liu

Graduate School of Maritime Sciences, Kobe Univ.

5-1-1, Fukae-minami, Kobe, Hyogo 658-0022, Japan

Takashi Nakajima

Institute of Advanced Energy, Kyoto Univ.

Gokasho, Uji, Kyoto 611-0011, Japan

ABSTRACT

Natural convection heat transfer from a vertical single cylinder with helical wire spacer in liquid sodium was numerically analyzed on the following four effects, the influences of surface heat flux, gap between helical wire and heated cylinder surface, pitch of helical wire and helical wire diameter on heat transfer. The unsteady laminar three dimensional basic equations for natural convection heat transfer caused by a step heat flux were numerically solved until the numerical solution reaches a steady-state. The PHOENICS code was used for the calculation considering the temperature dependence of thermo-physical properties concerned. The heated cylinder for diameter (D=7.6 mm), heated length (L=200 mm) and L/d (=26.32), and the helical wire spacers for gaps (0 to 1 mm), pitches (100 to 200 mm), helical wire diameters (d=1 to 2 mm) and height (H=470 mm) were used in this work. The surface heat fluxes

for each cylinder with helical wire spacer were equally given for a modified Rayleigh number, $(Ra_{f,L})_{w\text{-}s}$, ranging from 3.059×10^4 to 3.147×10^7 (q=1×10^4 to 7×10^6 W/m^2) in liquid temperature (T_L=673.15 K). The values of gap were given from 0 to 1 mm at d=1.2 mm and a pitch of 165 mm, those of pitch were given from 100 to 200 mm at d=1.2 mm and a gap of 0.2 mm and those of wire diameter were given from 1 to 2 mm at a gap of 0.2 mm and a pitch of 165 mm on each cylinder with helical wire spacer. The spatial distributions of local and average Nusselt numbers, $(Nu_{\theta,z})_{w\text{-}s}$ and $(Nu_{av})_{w\text{-}s}$, on each cylinder with helical wire spacer were clarified. The values of average Nusselt number, $(Nu_{av})_{w\text{-}s}$, for a vertical cylinder with helical wire spacer were calculated to examine the effects of $(Ra_{f,L})_{w\text{-}s}$, gap, pitch and helical wire diameter on heat transfer. The correlation for $(Nu_{av})_{w\text{-}s}$ for a vertical cylinder with helical wire spacer above mentioned including the effects of $(Ra_{f,L})_{w\text{-}s}$, gap, pitch and helical wire diameter was developed. The correlation can describe the theoretical values of $(Nu_{av})_{w\text{-}s}$ for a vertical cylinder with helical wire spacer within -2.74 to 1.63 % differences.

Key Words: Natural convection heat transfer, Vertical single cylinder, Helical wire spacer, Liquid sodium

1. Introduction

Knowledge of natural convection heat transfer from a vertical single cylinder with helical wire spacer in liquid sodium is important as a database for the natural circulation and the design of a heat exchanger in a fast reactor core for decay heat removal in the case of a loss of coolant accident (LOCA) and a loss of flow accident (LOFA). However, there has been published little fundamental experimental work from a vertical single cylinder and a vertical rod bundle with helical wire spacer in liquid sodium.

Research on a vertical rod bundle with helical wire spacer in liquid sodium has been conducted as follows. A forced flow inter-channel mixing model applicable to LMFBR fuel assemblies containing helical wire spacer systems that can be incorporated into COBRA-II and COBRA-III B lumped-parameter computer codes was presented by Ginsberg [1]. An investigation of the hydraulic behavior of wire-wrapped fuel and blanket assemblies in an air flow test facility was conducted by Roidt et al. [2]. Experimental results were discussed in detail below. 1. Static pressure gradients. 2. Local and average cross flow through the gap spacing between rods as a function of the wire wrap position and at all typical locations in the assembly. 3. Detailed axial velocity mappings in the inboard and peripheral channels. Ninokata et al. [3] have developed three-dimensional flow hydrodynamic distributed resistance models for

rod bundles. The models were tested against sub-channel velocity and temperature data taken from bundles of triangular rod array configurations with wire-spacers. Hu and Fanning [4] have developed a three-dimensional momentum source model (MSM) to model the anisotropic flow without the need to resolve the geometric details of the wire-wraps to improve the hydraulic modeling of wire-wrap spacers in a rod-bundle. Raj and Velusamy [5] have carried out RANS based computational fluid dynamic (CFD) simulation of flow and temperature fields in a sodium cooled fast reactor fuel subassembly which consists of 217 pins with helical wire spacers. Based on the investigation of transverse and axial flows in different types of sub-channels, correlations have been proposed for calculation of transverse flow, which forms an important input for development of sub-channel analysis codes. Zhao et al. [6] simulated transverse flow in a wire-wrapped hexagonal seven-pin bundle by computational fluid dynamic (CFD) method for reasons that transverse flow induced by helical spacer wires has important effects on the flow and heat transfer behavior of reactor core. Transverse velocity distributions in four different kinds of sub-channel gaps were analyzed and the influence of wire number and position on the transverse velocity distribution was clarified. Wang and Cheng [7] analyzed the flow field in a 19-rod bundle with wire wraps using the computational fluid dynamics (CFD) method for studying the characteristic of sweeping flow rate across the gaps between the sub-channels. The influence of the ratio of rod pitch (P) to rod diameter (D) on the velocity of the sweeping flow, and the influence of the ratio of wire pitch (H) to rod diameter (D) on the cross flow rate were clarified. A correlation as a function of both P/D ratio and H/D ratio was proposed to predict the sweeping flow velocity.

Recently, natural convection heat transfer from vertical 7×7 rod bundles without helical wire spacer in liquid sodium was numerically analyzed for the bundle geometry with equilateral square array, ESA. The unsteady laminar three dimensional basic equations for natural convection heat transfer caused by a step heat flux were numerically solved until the solution reaches a steady-state. The PHOENICS code was used for the calculation considering the temperature dependence of thermo-physical properties concerned. The 7×7 heated rods for diameter (D=7.6 mm), heated length (L=200 mm) and L/d (=26.32) were used in this work. The surface heat fluxes for each cylinder were equally given for a modified Rayleigh number, $(Ra_{f,L})_{ij}$ and $(Ra_{f,L})_{7\times7,S/D}$, ranging from 3.08×10^4 to 4.28×10^7 (q=1×10^4~7×10^6 W/m^2) in liquid temperature (T_L=673.15 K). The values of S/D, which are ratios of the diameter of flow channel for bundle geometry to the rod diameter, for vertical 7×7 rod bundles were ranged from 1.8 to 6 on the bundle geometry with equilateral square array. The spatial distribution of average Nusselt numbers for a vertical

single cylinder of a rod bundle, $(Nu_{av})_{ij}$, and average Nusselt numbers for a vertical rod bundle, $(Nu_{av,B})_{7\times7,S/D}$, were clarified. The average value of Nusselt number, $(Nu_{av})_{ij}$ and $(Nu_{av,B})_{7\times7,S/D}$, for the bundle geometry with various values of *S/D* were calculated to examine the effect of array size, bundle geometry, *S/D*, $(Ra_{f,L})_{ij}$ and $(Ra_{f,L})_{7\times7,S/D}$ on heat transfer. The bundle geometry for the higher $(Nu_{av,B})_{7\times7,S/D}$ value under the condition of *S/D*=constant was examined. The general correlations for natural convection heat transfer from a vertical *7×7* rod bundles with the equilateral square and triangle arrays including the effects of array size, $(Ra_{f,L})_{7\times7,S/D}$ and *S/D* were developed. The correlations for vertical *7×7* rod bundles can describe the theoretical values of $(Nu_{av,B})_{7\times7,S/D}$ for each bundle geometry in the wide analytical range of *S/D* (=1.8 to 6) and the modified Rayleigh number ($(Ra_{f,L})_{7\times7,S/D}$=$3.08\times10^4$ to 4.28×10^7) within -9.49 to 10.6 % differences [8-11].

The objectives of present study are: (1) to analyze theoretically natural convection heat transfer from a vertical single cylinder with helical wire spacer in liquid sodium to optimize the thermal-hydraulic design for the Vertical Rod Bundles with helical wire spacer, (2) to obtain the numerical solutions of local and average Nusselt numbers on a vertical single cylinder with helical wire spacer, $(Nu_{\theta,z})_{w\text{-}s}$ and $(Nu_{av})_{w\text{-}s}$, from theoretical laminar natural convection equations for wide ranges of heat flux, gap, pitch and helical wire diameter on a vertical single cylinder, (3) to clarify the effects of heat flux, gap, pitch and helical wire diameter on heat transfer, and (4) to derive general correlation for natural convection heat transfer from a vertical single cylinder with helical wire spacer to describe the effects of heat flux, gap, pitch and helical wire diameter on natural convection heat transfer.

2. Apparatus and method

The test vessel is shown schematically in Fig. 1 [8, 9, 12-15]. It is a cylindrical vessel of 288 mm in outer diameter and 470 mm in height containing liquid sodium of about 30.62 liter. A single heated cylinder of a *D* mm in diameter with helical wire spacer was mounted vertically at a central axis of the vessel. Natural convection heat transfer from a vertical single heated cylinder without helical wire spacer has been numerically analyzed [8, 9]. Natural convection heat transfers from a vertical single cylinder with helical wire spacer are also numerically analyzed for the various helical wire spacers as shown in Fig. 2. The various helical wire spacers are mounted vertically at even gap on circumference of diameter *D*+2×gap mm with a central axis of the vessel.

3. Theoretical solution of laminar natural convection equations

3.1 Fundamental equations

Considering the asymmetry of the problem, the unsteady laminar three-dimensional basic equations in cylindrical coordinates as shown in Fig. 2 for a vertical single cylinder with helical wire spacer are described as follows.

(Continuity Equation)

Cylindrical coordinates (θ, r, z)*:*

$$\frac{\partial \rho}{\partial t}+\frac{1}{r}\frac{\partial}{\partial r}\left(\rho r v_r\right)+\frac{1}{r}\frac{\partial}{\partial \theta}\left(\rho v_\theta\right)+\frac{\partial}{\partial z}\left(\rho v_z\right)=0 \tag{1}$$

(Momentum Equation)

θ-component:

$$\frac{\partial}{\partial t}\left(\rho v_\theta\right)+\frac{\partial}{\partial r}\left(\rho v_r v_\theta\right)+\frac{1}{r}\frac{\partial}{\partial \theta}\left(\rho v_\theta v_\theta\right)+\frac{\rho v_r v_\theta}{r}+\frac{\partial}{\partial z}\left(\rho v_z v_\theta\right)=-\frac{1}{r}\frac{\partial P}{\partial \theta}+\frac{1}{r^2}\frac{\partial}{\partial r}\left(r^2\tau_{r\theta}\right)+\frac{1}{r}\frac{\partial}{\partial \theta}\tau_{\theta\theta}+\frac{\partial}{\partial z}\tau_{\theta z}+\rho g_\theta \tag{2}$$

r-component:

$$\frac{\partial}{\partial t}\left(\rho v_r\right)+\frac{\partial}{\partial r}\left(\rho v_r v_r\right)+\frac{1}{r}\frac{\partial}{\partial \theta}\left(\rho v_\theta v_r\right)-\frac{\rho v_\theta^2}{r}+\frac{\partial}{\partial z}\left(\rho v_z v_r\right)=-\frac{\partial P}{\partial r}+\frac{1}{r}\frac{\partial}{\partial r}\left(r\tau_{rr}\right)+\frac{1}{r}\frac{\partial}{\partial \theta}\tau_{r\theta}-\frac{\tau_{\theta\theta}}{r}+\frac{\partial}{\partial z}\tau_{rz}+\rho g_r \tag{3}$$

z-component:

$$\frac{\partial}{\partial t}\left(\rho v_z\right)+\frac{\partial}{\partial r}\left(\rho v_r v_z\right)+\frac{1}{r}\frac{\partial}{\partial \theta}\left(\rho v_\theta v_z\right)+\frac{\partial}{\partial z}\left(\rho v_z v_z\right)=-\frac{\partial P}{\partial z}+\frac{1}{r}\frac{\partial}{\partial r}\left(r\tau_{rz}\right)+\frac{1}{r}\frac{\partial}{\partial \theta}\tau_{\theta z}+\frac{\partial}{\partial z}\tau_{zz}+\rho g_z \tag{4}$$

(Energy Equation)

Cylindrical coordinates (θ, r, z)*:*

$$\frac{\partial}{\partial t}\left(\rho c_p T\right)+\frac{\partial}{\partial r}\left(\rho c_p v_r T\right)+\frac{1}{r}\frac{\partial}{\partial \theta}\left(\rho c_p v_\theta T\right)+\frac{\partial}{\partial z}\left(\rho c_p v_z T\right)=\frac{1}{r}\frac{\partial}{\partial r}\left\{\frac{r\lambda}{c_p}\left(c_p\frac{\partial T}{\partial r}\right)\right\}+\frac{1}{r^2}\frac{\partial}{\partial \theta}\left\{\frac{\lambda}{c_p}\left(c_p\frac{\partial T}{\partial \theta}\right)\right\}+\frac{\partial}{\partial z}\left\{\frac{\lambda}{c_p}\left(c_p\frac{\partial T}{\partial z}\right)\right\} \tag{5}$$

Where $\tau_{rr}=2\rho\nu\frac{\partial v_r}{\partial r}$, $\tau_{\theta\theta}=2\rho\nu\left(\frac{1}{r}\frac{\partial v_\theta}{\partial \theta}+\frac{v_r}{r}\right)$, $\tau_{zz}=2\rho\nu\frac{\partial v_z}{\partial z}$ (6)

$$\tau_{r\theta}=\tau_{\theta r}=\rho\nu\left(r\frac{\partial}{\partial r}\left(\frac{v_\theta}{r}\right)+\frac{1}{r}\frac{\partial v_r}{\partial \theta}\right),\ \tau_{\theta z}=\tau_{z\theta}=\rho\nu\left(\frac{\partial v_\theta}{\partial z}+\frac{1}{r}\frac{\partial v_z}{\partial \theta}\right),\quad \tau_{zr}=\tau_{rz}=\rho\nu\left(\frac{\partial v_z}{\partial r}+\frac{\partial v_r}{\partial z}\right) \tag{7}$$

$$g_r=0,\quad g_\theta=0,\quad g_z=-g \tag{8}$$

and the v_θ, v_r and v_z are the θ, r and z-components of a velocity vector, respectively.

3.2 Boundary conditions

The calculation domain for asymmetry model of a cylindrical vessel of 288 mm in diameter and 470 mm in height were divided into (36, 34, 128) grid points for the θ, r, and z-components. And the first control volume width for r-component, Δr, on the heated section was given 0.4 mm as shown in Figs. 3 (a), (b) and (c) [8-11, 14, 15]. The time step, Δt, was set to 30 ms. The fundamental equations are numerically analyzed together with the following boundary conditions.

On the surfaces of cylinder: constant heat flux, and non-slip condition.

At the outer boundary of test vessel:

$$T = T_0, \quad \frac{\partial v_r}{\partial r} = 0 \qquad \text{for inflow} \qquad (9)$$

$$\frac{\partial \mathrm{T}}{\partial \mathrm{r}} = 0, \quad \frac{\partial \mathrm{v_r}}{\partial \mathrm{r}} = 0 \qquad \text{for outflow.} \qquad (10)$$

At the lower and upper boundary:

$$T = T_0, \quad \frac{\partial v_z}{\partial z} = 0 \qquad \text{for inflow} \qquad (11)$$

$$\frac{\partial T}{\partial z} = 0, \quad \frac{\partial v_z}{\partial z} = 0 \qquad \text{for outflow} \qquad (12)$$

where T_0 is a bulk liquid temperature at the initial condition.

3.3 Method of solution

The helical wire spacer 3D geometry data file was created using the SolidWorks 3D CAD Design Engineering Software Tool [16]. The coded 3D geometry data file was loaded into the PHOENICS-VR editor [17], and its dimensions and orientation were then converted into cylindrical coordinates. Simple shapes with rectangular and triangular facets formed by the helical wire spacer were combined to obtain the designed geometry. The object was represented by facets distributed on the outer surfaces of the object, as shown in Fig. 3 (c). The PARSOL function in PHOENICS is a technique that improves the accuracy of flow simulations for situations in which a fluid–solid boundary obliquely intersects some of the cells of a Cartesian or cylindrical coordinate grid, as shown in Figs. 3 (a), (b) and (c). PARSOL is capable of calculating fluid flow phenomena accurately, whether the flow is laminar or

turbulent, provided that the cell is cut by the interface into no more than two sub-cells, one containing fluid and the other solid. The control volume discretization equations were derived from these fundamental equations by using the hybrid scheme [18]. The thermo-physical properties for each control volume such as specific heat at constant pressure (c_p), thermal conductivity (λ), viscosity (μ) and density (ρ) are given as those at each volume temperature. The procedure for the calculation of the flow field is the SIMPLE algorithm which stands for Semi-Implicit Method for Pressure-Linked Equations.

The surface heat fluxes, q, for a vertical single cylinder with helical wire spacer were equally given in the value of 1×10^4 to 7×10^6 W/m^2 as an initial condition, and numerical calculation was continued until the steady-state was obtained. The surface temperature on the cylinder with helical wire spacer was calculated from the analyzed temperature of the first control volume on the cylinder surface, *TEM*, which is supposed to be located on the center of the control volume, by solving the thermal conduction equation in liquid sodium as follows [8-11, 14, 15].

$$T_s = \frac{q}{\lambda_l}\frac{\Delta r}{2} + TEM \tag{13}$$

where, Δr is the first control volume width for the r-component. In Fig. 4, the heated cylinder surface is located at r=0 mm and the conductive sub-layer [8-11, 19, 20] exists on the heated cylinder surface. The liquid temperatures in the conductive sub-layer on the heated cylinder surface will become linearly lower with an increase in the radius by the heat conduction from the surface temperature on the heated cylinder, $T_f=T_s-(q/\lambda_l)(\Delta r/2)$. And let those, T_f, equal the analyzed liquid temperature of the first control volume on the heated cylinder surface, *TEM*, as given in Eq. (13). Half the first control volume width for the r-component, $\Delta r/2$, would become the thickness of the conductive sub-layer, δ_{CSL}, for the local heat transfer on a vertical cylinder under two-phase model classified into laminar sub-layer and transition region of the buoyancy-driven flow. Average heat transfer coefficient on a cylinder surface with helical wire spacer was obtained by averaging the calculated 36 by 100 local surface temperatures on θ-axis and z-axis at every 10 degree and 2 mm, $\{(T_s)_{av}\}_{w\text{-}s}= \int_0^{100}\int_0^{36}\{(T_s)_{\theta,z}\}_{w\text{-}s}\, d\theta\, dz/(36\times100)$, in the peripheral angle, θ, of 360 degrees and the heated length, L, of 200 mm. All the calculations were made by using the PHOENICS code [18].

4. Results and discussion

In this section, the correlation of natural convection heat transfer from a vertical single cylinder without helical wire spacer previously obtained is first explained. The general correlation for vertical single cylinder with helical wire spacer is derived by the use of the following correlation for a vertical single cylinder without helical wire spacer.

4.1. Correlation for a vertical single cylinder without helical wire spacer (N=1) previously obtained [8, 9]

4.1.1. Local Nusselt number, Nu_z

The experimental data and the numerical solutions for liquid sodium and the numerical solutions for air are approximately expressed by the following correlation [8, 9, 21-23].

$$Nu_z = \left[1 + \frac{C}{\left(Ra_z^* \right)^{0.2}} \left(\frac{z}{D} \right)^{0.86} \right] Ra_f{}^{0.2} \tag{14}$$

where $C = 0.85 \left(\frac{Pr}{4 + 9Pr^{1/2} + 10Pr} \right)^{-0.2}$ (15)

$$Gr_z^* = \frac{g\beta qz^4}{\lambda \nu^2} \tag{16}$$

$$Ra_z^* = Gr_z^* Pr \tag{17}$$

$$Ra_{f,z} = \frac{Gr_z^* Pr^2}{4 + 9Pr^{1/2} + 10Pr} \tag{18}$$

In case of liquid sodium for liquid temperatures ranging from 673 to 873 K, C is constant ranging from 3.258 to 3.375 and almost equals to 3.36. The curves of Nu_z derived from the correlation, Eq. (14), are in agreement with the experimental data and the numerical solutions for vertical single cylinders without helical wire spacer within 20 % difference.

The experimental data of the local surface temperature rises, $(T_s)_z$-T_L, for a vertical single heated cylinder are shown versus the vertical distance from the leading edge of the heated section, z, as the black symbols in Fig. 5 for the heat fluxes, q, of 2×10^5, 7×10^5, 1×10^6 and 2×10^6 W/m^2 at liquid temperature of around 773 K. Numerical solutions numerically analyzed at the liquid temperatures of 773 K are also included as the red solid circles in the figure. At a fixed heat flux, q, the increasing rate of $(T_s)_z$-T_L is steep near the leading edge of the heated section and it becomes gradually gentle for z larger than 30 mm. The values obtained from Eq. (14) are also shown in the figure as

red broken lines for comparison. These temperature distributions are almost in good agreement with those for the experimental data and the numerical solutions on a vertical single cylinder within -14.91 to 18.25 % differences and -8.14 to -2.52 % ones.

4.1.2. Average Nusselt number, Nu_{av}

The average Nusselt number, Nu_{av}, for a vertical single cylinder without helical wire spacer is expressed from Eq. (14) as follows.

$$Nu_{av} = \left[\frac{1}{0.8} + \frac{C}{0.86\left(Ra_L^*\right)^{0.2}} \left(\frac{L}{D} \right)^{0.86} \right] Ra_{f,L}{}^{0.2} \tag{19}$$

where $Ra_L^* = Gr_L^* Pr$ (20)

$$Gr_L^* = \frac{g\beta q L^4}{\lambda \nu^2} \tag{21}$$

$$Ra_{f,L} = \frac{Gr_L^* Pr^2}{4 + 9Pr^{1/2} + 10Pr} \tag{22}$$

The values of the average Nusselt number, Nu_{av}, derived from the correlation, Eq. (19), on a vertical single heated cylinder of 7.6 mm in diameter and 200 mm in heated length become 41.502 and 45.511 for the heat fluxes, q, of 1×10^6 and 2×10^6 W/m^2 at the liquid temperature of 673.15 K, and 42.386 and 46.576 for the heat fluxes, q, of 1×10^6 and 2×10^6 W/m^2 at the liquid temperature of 773.15 K, respectively.

4.1.3. Thickness of conductive sub-layer on natural convection, δ_{CSL}

The typical example of the laminar natural convection heat transfer curve for vertical cylinder, D, of 7.62 mm, heated length, L, of 186 mm and heated length-to-cylinder diameter ratios, L/d, of 24.41 without helical wire spacer at the liquid temperature, T_L, of around 773.15 K is plotted versus the temperature difference between average inner surface temperature and liquid bulk mean temperature, ΔT_L ($=T_{s,av}-T_L$), in Fig. 6. The numerical solutions for the relation between the heat flux, q, and the temperature difference between average inner surface temperature and liquid bulk mean temperature, ΔT_L, are shown as green solid circles. The numerical solutions of the theoretical equations for laminar natural convection are in good agreement with the experimental data and the values derived from Eq. (19) within -15 % differences as shown in Fig. 6. The thicknesses of the conductive sub-layer, δ_{CSL}, for the

laminar natural convection heat transfer on the vertical cylinder of D=7.62 mm and L=186 mm in Fig 6 is 200 μm. The thickness of the conduction sub-layer does not depend on the heat flux and is almost constant at 200 μm in the wide ΔT_L region.

4.2. Local heat transfer for a vertical single cylinder with helical wire spacer

Natural convection heat transfers from a vertical single cylinder with helical wire spacer are numerically analyzed for the geometry as shown in Fig. 2. The heated cylinder for diameter (D=7.6 mm), heated length (L=200 mm) and L/d (=26.32) and helical wire spacers for gap (0 to 1 mm), pitch (100 to 200 mm), diameter (d=1 to 2 mm) and height (H=470 mm) were given in this work. The surface heat fluxes for each cylinder with helical wire spacer were equally given at 1×10^4, 2×10^4, 7×10^4, 1×10^5, 2×10^5, 7×10^5, 1×10^6, 2×10^6 and 7×10^6 W/m^2. The parameters used for calculation were tabulated in Table 1.

4.2.1. Effects of helical wire spacer, peripheral angle and heat flux on heat transfer

The numerical solutions of local surface temperature rises, $\{(T_s)_{\theta,z}\}_{w\text{-}s}$-$T_L$, for a vertical single cylinder with helical wire spacer are shown versus the vertical distance from the leading edge of the heated section, z, in Figs. 7 [peripheral angle, θ=5 to 175 degrees (ix=1 to 18)] and 8 [θ=185 to 355 degrees (ix=19 to 36)] for the liquid temperature of about 673 K and the heat fluxes, q, of 2×10^5, 1×10^6 and 2×10^6 W/m^2 with helical wire spacer for gap (0.2 mm), pitch (165 mm), diameter (d=1.2 mm) and height (H=470 mm). The peripheral angle was divided into 36 every 10 degrees as shown in Fig. 3 (a). The peripheral angles of the heated cylinder, θ, correspond to 5, 85, 175, 265 and 355 degrees from top on the vertical axis for the ix of 1, 9, 18, 27 and 36 respectively.

The numerical results of the local surface temperature, $\{(T_s)_{\theta,z}\}_{w\text{-}s}$, the local Nusselt number, $(Nu_{\theta,z})_{w\text{-}s}$, and the modified Rayleigh number, $\{(Ra_{f,L})_{\theta,z}\}_{w\text{-}s}$, for a vertical single cylinder with helical wire spacer were obtained as follows:

$$\{(T_s)_{\theta,z}\}_{w-s}=[\{T_s(z)\}_\theta]_{w-s} \tag{23}$$

$$(Nu_{\theta,z})_{w-s}=\frac{(h_{\theta,z})_{w-s}\times z}{\lambda_l}=\frac{q\times z}{\lambda_l[\{(T_s)_{\theta,z}\}_{w-s}-T_L]} \tag{24}$$

$$\{(Ra_f)_{\theta,z}\}_{w-s}=\frac{\{(Gr^*)_{\theta,z}\}_{w-s}\{(Pr)_{\theta,z}\}^2_{w-s}}{4+9\{(Pr)_{\theta,z}\}^{1/2}_{w-s}+10\{(Pr)_{\theta,z}\}_{w-s}} \tag{25}$$

At a fixed heat flux, q, the local surface temperature rise for θ=5° (ix=1, red solid line) becomes higher with increasing z as shown in the figure. The increasing rate of $\{(T_s)_{\theta,z}\}_{w\text{-}s}$-$T_L$ is steep near the leading edge of the heated section and it becomes gradually gentle for z larger than 30 mm. The temperature distribution is almost in good agreement with that for a vertical single cylinder without helical wire spacer. The increasing rate of $\{(T_s)_{\theta,z}\}_{w\text{-}s}$-$T_L$ rises suddenly again at z=83 mm in the presence of helical wire spacer on the control volume of the calculation mesh (due to narrow gap heat transfer), the local surface temperature rises peak at z=89 mm, subsequently decreases to a minimum at z=112 mm and it gradually increases with increasing z. The surface temperature after exceeding the presence of helical wire spacer becomes a little lower than the value for a vertical single cylinder without helical wire spacer (due to disturbance of buoyancy driven flow). When the peripheral angle and ix increase by 10 degrees and 1 each time, the values of the position z of the point where the rise begins, the peak point and the descent point increase by about 4.58 mm. The sharp rise in the increase rate occurs at a constant interval distance, Δz, as the peripheral angle increases. The rapid increase in the rate of increase becomes greater as the heat flux increases as shown in figures.

The contours of liquid temperature of the r-z plane on θ=105° and the r-θ plane on z=25, 99 and 199 mm from the leading edge of the heated section for a vertical single cylinder with helical wire spacer (d=1.2 mm, gap=0.2 mm and pitch=165 mm) at q=1×10^6 W/m^2 were plotted in Figs. 9 (a) and (b). It is recognized that the liquid temperatures around the circumference on the heated section for a vertical single cylinder with helical wire spacer become lower and higher with increases in the radius, r, and the vertical distance from the leading edge of the heated section, z, respectively, as mentioned in a former article [9-11].

The numerical solutions of $(v_\theta)_{w\text{-}s}$, $(v_r)_{w\text{-}s}$ and $(v_z)_{w\text{-}s}$ on the first control volume (r=3.8 mm) for a vertical single cylinder with helical wire spacer (d=1.2 mm, gap=0.2 mm and pitch=165 mm) are shown versus the vertical distance from the leading edge of the heated section, z, at various peripheral angles (θ=45°, 135°, 225° and 315°) with q =1×10^6 W/m^2 in Fig. 10. The $(v_\theta)_{w\text{-}s}$, $(v_r)_{w\text{-}s}$ and $(v_z)_{w\text{-}s}$ are plotted with broken lines, one dot dashed ones and solid ones for each color with respect to the peripheral angle, respectively. The numerical solutions of v_θ, v_r and v_z on the first control volume for a vertical single cylinder without helical wire spacer are shown in the figure for comparison as the black solid line with open circle, open triangle and solid circle [8, 9]. In the lower part of the figure, the numerical solutions of local surface temperature rises, $\{(T_s)_{\theta,z}\}_{w\text{-}s}$-$T_L$, for a vertical single cylinder with helical wire

spacer are also plotted with solid lines for each color with respect to the peripheral angle at peripheral angles, θ, of 45°, 135°, 225° and 315°, and those without helical wire spacer are plotted by black solid line with red solid circle. The numerical solutions of $(v_\theta)_{w\text{-}s}$, $(v_r)_{w\text{-}s}$ and $(v_z)_{w\text{-}s}$ at the peripheral angle of 45° (sky-blue solid curve) almost agree with the values of v_θ, v_r and v_z for a vertical single cylinder without helical wire spacer up to about 28 mm before the presence of a helical wire spacer (z=79 mm). The $(v_z)_{w\text{-}s}$ begins to decrease and recovers once, but it starts sudden decrease again from 10 mm before the presence of helical wire spacer (z=96 mm) and reaches the minimum value $(v_z)_{w\text{-}s}$=0.023 m/s at the helical wire spacer position (z=106 mm). After that, the $(v_z)_{w\text{-}s}$ turns to rise with an increase in the heated length, crosses the value of v_z for a vertical single cylinder without helical wire spacer at 13 mm behind the presence of helical wire spacer (z=119.6 mm), reaches the maximum value $(v_z)_{w\text{-}s}$=0.0776 m/s at the 47.4 mm behind the presence of helical wire spacer (z=154 mm), and gradually decreases. The values of $(v_\theta)_{w\text{-}s}$ and $(v_r)_{w\text{-}s}$ fluctuate with decrease and increase of $(v_z)_{w\text{-}s}$, but these fluctuation range are not as large as $(v_z)_{w\text{-}s}$. It can be concluded that the sharp rises in local surface temperature rise, $\{(T_s)_{\theta,z}\}_{w\text{-}s}$-$T_L$, for a vertical single cylinder with helical wire spacer (sky-blue solid curve) as shown in the lower diagram of Fig. 10 are based on the sharp decreases in the buoyancy-driven flow $(v_z)_{w\text{-}s}$ due to blocking flow by the presence of helical wire spacer.

The local Nusselt numbers, $(Nu_{\theta,z})_{w\text{-}s}$, for a vertical single cylinder with helical wire spacer (d=1.2 mm, gap=0.2 mm and pitch=165 mm) at various peripheral angles of the heated cylinder [θ=5 to 175 degrees (ix=1 to 18) and θ=185 to 355 degrees (ix=19 to 36)] are plotted versus the vertical distance from the leading edge of the heated section, z, in Figs. 11 and 12 for the liquid temperature of about 673 K and the heat fluxes, q, of 2×10^5, 1×10^6 and 2×10^6 W/m^2, respectively.

At a fixed heat flux, q, the local Nusselt numbers, $(Nu_{\theta,z})_{w\text{-}s}$, at θ=5° (ix=1, red solid line) become linearly higher with increasing z as shown in the figure. These $(Nu_{\theta,z})_{w\text{-}s}$ distributions are almost in good agreement with those for vertical single cylinder without helical wire spacer. The local Nusselt number rapidly decreases when there is the presence of helical wire spacer on the control volumes of the calculation mesh (due to narrow gap heat transfer), and when the wire spacer does not exist in the control volume, the local Nusselt number rises again. However, the value is somewhat larger than the local Nusselt number for a vertical single cylinder without helical wire spacer (due to disturbance of buoyancy driven flow). The rapid decrease in the rate of decrease becomes greater as the heat flux increases as shown in figures. The local Nusselt numbers, $(Nu_{\theta,z})_{w\text{-}s}$, also decrease with the decrease in the heat flux,

q, for the whole range of the vertical distance from the leading edge of the heated section, *z*, analyzed here.

5. Correlation for a vertical single cylinder with helical wire spacer

The numerical solutions were numerically analyzed natural convection heat transfer from a vertical single cylinder with helical wire spacers for gaps (0 to 1 mm), pitches (100 to 200 mm), diameters (d=1 to 2 mm) and height (H=470 mm). In this section the correlation for a vertical single cylinder with helical wire spacer including the effects of $(R_{f,L})_{w\text{-}s}$, gap, pitch and helical wire diameter on heat transfer is derived based on the numerical solutions.

5.1. Calculated results of $(Nu_{av})_{w\text{-}s}$ for a vertical single cylinder with helical wire spacer

Numerical solutions of average heat transfer coefficients from a vertical single cylinder with helical wire spacer (d=1.2 mm, gap=0.2 mm and pitch=165 mm) are plotted on $(Nu_{av})_{w\text{-}s}$ vs. $(Ra_{f,L})_{w\text{-}s}$ graph in Fig. 13. The average Nusselt number, $(Nu_{av})_{w\text{-}s}$, and the modified Rayleigh number, $(Ra_{f,L})_{w\text{-}s}$, for a vertical single cylinder with helical wire spacer were obtained as follows:

$$\{(T_s)_{av}\}_{w-s} = \frac{\sum_{i=1}^{N_\theta}\sum_{j=1}^{N_z}\{(T_s)_{i,j}\}_{w-s}}{(N_\theta \times N_z)} \tag{26}$$

$$(Nu_{av})_{w-s} = \frac{h \times L}{\lambda_l} = \frac{q \times L}{\lambda_l \times [\{(T_s)_{av}\}_{w-s} - T_L]} \tag{27}$$

$$(Ra_{f,L})_{w-s} = \frac{(Gr_L^*)_{w-s}(Pr)_{w-s}^2}{4 + 9(Pr)_{w-s}^{1/2} + 10(Pr)_{w-s}} \tag{28}$$

The calculation domain for asymmetry model of a heated cylindrical surface with helical wire spacer were divided into N_θ=36 and N_z=100 grid points for the θ and z-components. The numerical solutions for a vertical single cylinder with helical wire spacer (d=1.2 mm, gap=0.2 mm and pitch=165 mm) are shown as black cross symbols in the figure. The surface heat fluxes for a vertical single cylinder with helical wire spacer were equally given at 1×10^4, 2×10^4, 7×10^4, 1×10^5, 2×10^5, 7×10^5, 1×10^6, 2×10^6 and 7×10^6 W/m^2 and the values of $(Ra_{f,L})_{w\text{-}s}$ at that time are 3.059×10^4, 6.123×10^4, 2.150×10^5, 3.081×10^5, 6.200×10^5, 2.235×10^6, 3.248×10^6, 6.860×10^6 and 3.147×10^7, respectively. The numerical solutions, Nu_{av}, for a vertical single cylinder without helical wire spacer are shown in the figure for comparison as the black open circles [8, 9]. The Nu_{av} values for a vertical single cylinder without helical wire spacer predicted by Eq. (19) are also shown in the figure as the red open circles and a red broken curve. As can

be seen in the figure, the numerical solution of $(Nu_{av})_{w\text{-}s}$ for a vertical single cylinder with helical wire spacer is about 6.67 % lower than the value calculated by Eq. (19) for the vertical single cylinder without helical wire spacer at the $(Ra_{f,L})_{w\text{-}s}$ of 3.057×10^4 (q=1×10^4 W/m^2). Those become also linearly higher with an increase in the $(Ra_{f,L})_{w\text{-}s}$ in parallel with Nu_{av} for a vertical single cylinder without helical wire spacer. The numerical solutions of $(Nu_{av})_{w\text{-}s}$ for a vertical single cylinder with helical wire spacer are almost in better agreement with those of Nu_{av} for a vertical single cylinder without helical wire spacer in the whole range of the modified Rayleigh number, $(Ra_{f,L})_{w\text{-}s}$, and those with and without helical wire spacer can be expressed by authors' correlation for a vertical single cylinder without helical wire spacer, Eq. (19), within 10 % differences.

5.1.1. Comparison of analytical solutions of $(Nu_{av})_{w\text{-}s}$ with authors' correlation, Eq. (19)

The numerical solutions for a vertical single cylinder with helical wire spacer are compare with authors' correlation for a vertical single cylinder without helical wire spacer, Eq. (19), in Fig. 14. The ratios of the numerical solutions for a vertical single cylinder with helical wire space to the values given by authors' correlation, Eq. (19), are plotted as the black cross symbols on $(Nu_{av})_{w\text{-}s}/(Nu_{av})_{Eq.(19)}$ versus $(Ra_{f,L})_{w\text{-}s}$ graph in Fig. 14. Furthermore, those of the numerical solutions for a vertical single cylinder without helical wire spacer to the values given by Eq. (19) are shown as the black open circles in the figure. The ratios of $(Nu_{av})_{w\text{-}s}$ to $(Nu_{av})_{Eq.(19)}$ and those of $Nu_{av}/(Nu_{av})_{Eq.(19)}$ are approximately given by the following correlations.

$$\frac{\left(Nu_{av}\right)_{w-s}}{\left(Nu_{av}\right)_{Eq.(19)}} = C_1 \times \left(Ra_{f,L}\right)_{w-s}^{n} = 0.8704 \times \left(Ra_{f,L}\right)_{w-s}^{0.003095} \tag{29}$$

$$\frac{Nu_{av}}{\left(Nu_{av}\right)_{Eq.(19)}} = C_1 \times Ra_{f,L}^{n} = 0.7786 \times Ra_{f,L}^{0.0121} \tag{30}$$

Equations, Eqs. (29) and (30), for a vertical single cylinder with and without helical wire spacer are in good agreement with the ratios of $(Nu_{av})_{w\text{-}s}$ to $(Nu_{av})_{Eq.(19)}$ within -2.75 to 1.63 % differences as well as those of $Nu_{av}/(Nu_{av})_{Eq.(19)}$ within -1.50 to 1.63 % differences. These equations including a vertical single cylinder without helical wire spacer, Eq. (19), would become the general correlations for average Nusselt number versus modified Rayleigh number, $(Nu_{av})_{w\text{-}s}=f\{(Ra_{f,L})_{w\text{-}s}\}$, on a vertical single cylinder with and without helical wire spacer.

5.2. Effect of gap on $(Nu_{\theta,z})_{w\text{-}s}$ and $(Nu_{av})_{w\text{-}s}$

Natural convection heat transfer for a vertical single cylinder with helical wire spacer (d=1.2 mm and pitch=165 mm) were numerically analyzed to examine the effect of gap on local and average Nusselt numbers at the constant heat flux condition of $(Ra_{f,L})_{w\text{-}s}=3.248\times10^6$ ($q=1\times10^6$ W/m^2) for gaps ranging from 0 mm to 1 mm. Typical numerical solutions of the local surface temperature rise, $\{(T_s)_{\theta,z}\}_{w\text{-}s}\text{-}T_L$, and the local Nusselt number, $(Nu_{\theta,z})_{w\text{-}s}$, for a vertical single cylinder with helical wire spacer (d=1.2 mm, gap=0.6 mm and pitch=165 mm) are shown against the vertical distance from the leading edge of the heated section, z, in Figs. 15 to 18 for the liquid temperature of about 673 K and the heat flux, q, of 1×10^6 W/m^2. The gap width is gap=0.6 mm which is three times larger than the gap=0.2 mm shown in Figs. 7, 8, 11 and 12. The sharp increase in the rate of increase in Figs. 15 and 16 becomes smaller as the gap increases as compared with Fig. 7 and 8. The abrupt decrease in the reduction rate in Figs. 17 and 18 becomes smaller as the gap increases as compared with Fig. 11 and 12. Numerical solutions of average Nusselt numbers from a vertical single cylinder with helical wire spacer (d=1.2 mm, gap=0 to 1 mm and pitch=165 mm) are plotted on $(Nu_{av})_{w\text{-}s}$ vs. gap graph in Fig. 19. The numerical solutions of $(Nu_{av})_{w\text{-}s}$ are almost constant in the analysis range from 0 to 1 mm in gap as shown in Fig. 19, which are 0.876% to 2.32% smaller than those of Nu_{av} for a vertical single cylinder without helical wire spacer as shown in Fig. 20.

5.3. Effect of pitch on $(Nu_{\theta,z})_{w\text{-}s}$ and $(Nu_{av})_{w\text{-}s}$

The numerical solutions of natural convection heat transfer for a vertical single cylinder with helical wire spacer (d=1.2 mm gap=0.2 mm and pitch=100 mm) were plotted in Figs. 21 to 24 to investigate the effect of pitch on local and average Nusselt numbers for pitch ranging from 100 to 200 mm at the constant heat flux condition of $(Ra_{f,L})_{w\text{-}s}=3.248\times10^6$ ($q=1\times10^6$ W/m^2). When the peripheral angle and ix increase by 10 degrees and 1 each time, the values of the position z of the point where the rise begins, the peak point and the descent point increased by about 2.78 mm. As shown in Figures 21 to 24, it is observed that the sharp rises in the increase rate in the local temperature of $\{(T_s)_{\theta,z}\}_{w\text{-}s}\text{-}T_L$ and a noticeable drops in the local Nusselt number of $(Nu_{\theta,z})_{w\text{-}s}$ occur exactly twice at each peripheral angle of 10 degrees in the heated section 200 mm range. The average Nusselt numbers, $(Nu_{av})_{w\text{-}s}$, become almost constant even at pitch ranging from 100 mm more to 200 mm as shown in Fig. 25. These are almost identical with the

average Nusselt number for a vertical single cylinder without helical wire spacer, Nu_{av}, within -2.74 to -2.34 % differences as shown in Fig. 26.

5.4. Effect of wire diameter on $(Nu_{\theta,z})_{w\text{-}s}$ and $(Nu_{av})_{w\text{-}s}$

The local surface temperature rises, $\{(T_s)_{\theta,z}\}_{w\text{-}s}\text{-}T_L$, for a vertical single cylinder with helical wire spacer (d=1.6 mm, gap=0.2 mm and pitch=165 mm) are shown versus the vertical distance from the leading edge of the heated section, z, in Figs. 27 and 28 for the liquid temperature of about 673 K and the heat flux, q, of 1×10^6 W/m^2 to clarify the effect of wire diameter on heat transfer. The local Nusselt number, $(Nu_{\theta,z})_{w\text{-}s}$, for a vertical single cylinder with helical wire spacer (d=1.6 mm, gap=0.2 mm and pitch=165 mm) are shown versus the vertical distance from the leading edge of the heated section, z, in Figs. 29 and 30. The local surface temperature rise distribution in Figs. 27 and 28 and the local Nusselt number distribution in Figs. 29 and 30 are almost the same as those in Figs. 7 and 8 and those in Figs. 11 and 12 with a wire diameter, d, of 1.2 mm. The effect of d on average Nusselt numbers, $(Nu_{av})_{w\text{-}s}$, was estimated based on the numerical solutions for the d ranging from 1 to 2 mm. The calculations were made for the heat flux, q, of 1×10^6 W/m^2. The $(Nu_{av})_{w\text{-}s}$ are shown versus d in Fig. 31 with Nu_{av} and Eq. (19). As can be seen in these figure, the values of $(Nu_{av})_{w\text{-}s}$ for the heat flux of 1×10^6 W/m^2 become linearly lower with an increase in d for the d ranging from 1 to 2 mm and these seem to be almost constant values. The values of $(Nu_{av})_{w\text{-}s}$ almost agree with the tendency of d with respect to Nu_{av} for a vertical single cylinder without helical wire spacer, which are 2.00 to 4.59 % smaller than Nu_{av} as shown in Fig. 32.

5.5. General correlation for natural convection heat transfer from a vertical single cylinder with helical wire spacer

In the numerical analysis of a vertical single cylinder with helical wire spacer, it was found that influences of heat flux, gap, pitch and wire diameter on the local and average Nusselt numbers, $(Nu_{\theta,z})_{w\text{-}s}$ and $(Nu_{av})_{w\text{-}s}$, hardly existed as described above.

The widely and precisely predictable correlation of natural convection heat transfer from a vertical single cylinder with helical wire spacer in liquid sodium was given by substituting Eq. (19) for Nu_{av} in Eq. (29) based on the numerical solutions.

$$\left(Nu_{av}\right)_{w-s} = C_1 \times \left(Ra_{f,L}\right)_{w-s}^{n} \times \left[\frac{1}{0.8} + \frac{C}{0.86\left\{\left(Ra_L^*\right)_{w-s}\right\}^{0.2}}\left(\frac{L}{D}\right)^{0.86}\right]\left(Ra_{f,L}\right)_{w-s}^{0.2} \quad (31)$$

$$C_1 = 0.8704 \quad (32)$$

$$n = 0.003095 \quad (33)$$

The curves given by Eq. (31) for a vertical single cylinder with helical wire spacer are shown as the blue solid line in Fig. 13 at each $(Ra_{f,L})_{w\text{-}s}$ for comparison. The numerical solutions are in good agreement with the values given by the correlation, Eq. (31), within -2.74 to 1.63 % differences.

6. Conclusions

Natural convection heat transfer from a vertical single cylinder with helical wire spacer in liquid sodium was numerically analyzed to clarify the influences of surface heat flux, gap, pitch and helical wire diameter on heat transfer. The heated cylinder for diameter (D=7.6 mm), heated length (L=200 mm) and L/d (=26.32) and helical wire spacers for gaps (0 to 1 mm), pitches (100 to 200 mm), wire diameters (d=1 to 2 mm) and height (H=470 mm) were used in this work. The surface heat fluxes for each cylinder with helical wire spacer were equally given for a modified Rayleigh number, $(Ra_{f,L})_{w\text{-}s}$, ranging from 3.059×10^4 to 3.147×10^7 (q=1×10^4 to 7×10^6 W/m^2) in liquid temperature (T_L=673.15 K). Numerical solutions lead to the following conclusions.

1) The increasing rate of $\{(T_s)_{\theta,z}\}_{w\text{-}s}$-$T_L$ rises suddenly again in the presence of helical wire spacer on the control volume of the calculation mesh (due to narrow gap heat transfer), the local surface temperature rises peak, subsequently decreases to a minimum and it gradually increases with increasing z. The surface temperature after exceeding the presence of helical wire spacer becomes a little lower than the value for a vertical single cylinder without helical wire spacer (due to disturbance of buoyancy driven flow). The rapid increase in the rate of increase becomes greater as the heat flux increases.
2) It can be concluded that the sharp rises in local surface temperature rise, $\{(T_s)_{\theta,z}\}_{w\text{-}s}$-$T_L$, for a vertical single cylinder with helical wire spacer are based on the sharp decreases in the buoyancy-driven flow $(v_z)_{w\text{-}s}$ due to blocking flow by the presence of helical wire spacer.

3) The local Nusselt number rapidly decreases when there is the presence of helical wire spacer on the control volume of the calculation mesh (due to narrow gap heat transfer), and when the wire spacer does not exist in the control volume, the local Nusselt number rises again. However, the value is somewhat larger than the local Nusselt number for a vertical single cylinder without helical wire spacer (due to disturbance of buoyancy driven flow). The rapid decrease in the rate of decrease becomes greater as the heat flux increases.

4) The numerical solution of $(Nu_{av})_{w\text{-}s}$ for a vertical single cylinder with helical wire spacer is about 6.67 % lower than the value calculated by Eq. (19) for the vertical single cylinder without helical wire spacer at the $(Ra_{f,L})_{w\text{-}s}$ of 3.057×10^4 (q=1×10^4 W/m^2). Those become also linearly higher with an increase in the $(Ra_{f,L})_{w\text{-}s}$ in parallel with Nu_{av} for a vertical single cylinder without helical wire spacer.

5) Numerical solutions of average Nusselt numbers from a vertical single cylinder with helical wire spacer (d=1.2 mm, gap=0 to 1 mm and pitch=165 mm) are almost constant in the analysis range from 0 to 1 mm in gap, which are 0.876% to 2.32% smaller than the numerical solutions of Nu_{av} for a vertical single cylinder without helical wire spacer.

6) The average Nusselt numbers, $(Nu_{av})_{w\text{-}s}$, become almost constant even at pitch ranging from 100 mm more to 200 mm. These are almost identical with the average Nusselt number for a vertical single cylinder without helical wire spacer, Nu_{av}, within -2.74 to -2.34 % differences.

7) The values of $(Nu_{av})_{w\text{-}s}$ for the heat flux of 1×10^6 W/m^2 become linearly lower with an increase in d for the d ranging from 1 to 2 mm. The values of $(Nu_{av})_{w\text{-}s}$ almost agree with the tendency of d with respect to Nu_{av} for a vertical single cylinder without helical wire spacer, which is 2.00 to 4.59 % smaller than Nu_{av}.

8) The numerical solutions are in good agreement with the values given by the widely and precisely predictable correlation of natural convection heat transfer from a vertical single cylinder with helical wire spacer in liquid sodium, Eq. (31), within -2.74 to 1.63 % differences.

Nomenclature

C parameter in Eqs. (14) and (19)

C_1 constant in Eqs. (29), (30) and (31)

c_p specific heat at constant pressure, J/kg K

D cylinder diameter and rod diameter, m

d helical wire diameter, m

Gr_L^* $= g\,\beta_l\,q\,L^4/\lambda_l\,\nu_l^2$, Grashof number for constant heat flux without helical wire spacer

$(Gr_L^*)_{w\text{-}s}$ $= g\,\beta_l\,q\,L^4/\lambda_l\,\nu_l^2$, Grashof number for constant heat flux with helical wire spacer

Gr_z^* $= g\,\beta_l\,q\,z^4/\lambda_l\,\nu_l^2$, local Grashof number for constant heat flux without helical wire spacer

$(Gr_z^*)_{w\text{-}s}$ $= g\,\beta_l\,q\,z^4/\lambda_l\,\nu_l^2$, local Grashof number for constant heat flux with helical wire spacer

g acceleration of gravity, m/s^2

H height, m

h_{av} average heat transfer coefficient for a vertical single cylinder without helical wire spacer, W/(m^{2}K)

$(h_{av})_{w\text{-}s}$ average heat transfer coefficient for a vertical single cylinder with helical wire spacer, W/(m^{2}K)

h_z local heat transfer coefficient for a vertical single cylinder without helical wire spacer, W/(m^{2}K)

$(h_z)_{w\text{-}s}$ local heat transfer coefficient for a vertical single cylinder with helical wire spacer, W/(m^{2}K)

L heated length, m

N_r grid point for the r-component

N_z grid point for the z-component

N_θ grid point for the θ-component

n exponent in Eqs. (29), (30) and (31)

Nu Nusselt number

Nu_{av} average Nusselt number for a vertical single cylinder without helical wire spacer

$(Nu_{av})_{w\text{-}s}$ average Nusselt number for a vertical single cylinder with helical wire spacer

Nu_z $=q\,z/\lambda_l\,(T_S\text{-}T_L)$, local Nusselt number for a vertical cylinder without helical wire spacer

$Nu_{\theta,z}$ $=q\,z/\lambda_l\,(T_S\text{-}T_L)$, local Nusselt number for a vertical cylinder without helical wire spacer at peripheral angle of the heated cylinder, θ

$(Nu_{\theta,z})_{w\text{-}s}$ $=q\,z/\lambda_l\,(T_S\text{-}T_L)$, local Nusselt number for a vertical cylinder at peripheral angle of the heated cylinder, θ

Pr $=c_{pl}\,\mu_l/\lambda_l$, Prandtl number

q heat flux, W/m^2

Ra_L^* $= Gr_L^*Pr$, Rayleigh number for constant heat flux without helical wire spacer

$(Ra_L^*)_{w\text{-}s} = Gr_L^*Pr$, Rayleigh number for constant heat flux with helical wire spacer

Ra_z^* = Gr_z^*Pr, local Rayleigh number for constant heat flux without helical wire spacer

$(Ra_z^*)_{w\text{-}s}$ = Gr_z^*Pr, local Rayleigh number for constant heat flux with helical wire spacer

$Ra_{f,z}$ = $Gr_z^*Pr^2/(4+9Pr^{1/2}+10Pr)$, modified local Rayleigh number without helical wire spacer

$\{(Ra_f)_{\theta,z}\}_{w\text{-}s}$ = $Gr_z^*Pr^2/(4+9Pr^{1/2}+10Pr)$, modified local Rayleigh number with helical wire spacer

$Ra_{f,L}$ = $Gr_L^*Pr^2/(4+9Pr^{1/2}+10Pr)$, modified Rayleigh number without helical wire spacer

$(Ra_{f,L})_{w\text{-}s}$ = $Gr_L^*Pr^2/(4+9Pr^{1/2}+10Pr)$, modified Rayleigh number with helical wire spacer

r radius of a cylinder, m

Δr first control volume width for r-component, m

T temperature, K and °C

TEM analyzed liquid temperature of the first control volume, K

T_f liquid temperature, K

T_L bulk liquid temperature, K

T_s heater surface temperature, K

$(T_s)_{av}$ average surface temperature without helical wire spacer, K

$\{(T_s)_{av}\}_{w\text{-}s}$ average surface temperature with helical wire spacer, K

$(T_s)_z$ local surface temperature without helical wire spacer, K

$\{(T_s)_{\theta,z}\}_{w\text{-}s}$ local surface temperature with helical wire spacer, K

Δt time step, s

z cylinder height and the vertical distance from the leading edge of the heated section, m

β volumetric expansion coefficient, K^{-1}

θ peripheral angle from inside on the r-θ plane, degree

λ thermal conductivity, W/(m K)

μ viscosity, Ns/m^2

v kinematic viscosity, m^2/s

ρ density, kg/m^3

Subscript

l liquid

Acknowledgments

This work was supported by the "Joint Usage/Research Program on Zero-Emission Energy Research, Institute of Advanced Energy, Kyoto University, Japan, ZE30B-03, 2018."

References

[1] Ginsberg, T., Forced-flow inter-channel mixing model for fuel rod assemblies utilizing a helical wire-wrap spacer system, Nuclear Engineering and Design, Vol. 22 (1972), pp. 38-42.

[2] Roidt, R.M., Carelli M.D., and Markley, R.A., Experimental investigations of the hydraulic field in wire-wrapped LMFBR core assemblies, Nuclear Engineering and Design, Vol. 62 (1980), pp. 295-321.

[3] Ninokata, H. Efthimiadis, A. and Todreas, N.E., Distributed resistance modeling of wire-wrapped rod bundles, Nuclear Engineering and Design, Vol. 104 (1987), pp. 93-102.

[4] Hu, Rui and Fanning, T.H., A momentum source model for wire-wrapped rod bundles—Concept, validation, and application, Nuclear Engineering and Design, Vol. 262 (2013), pp. 371-389.

[5] Raj, M.N. and Velusamy, K., Characterization of velocity and temperature fields in a 217 pin wire wrapped fuel bundle of sodium cooled fast reactor, Annuls of Nuclear Energy, Vol. 87 (2016), pp. 331-349.

[6] Zhao, P., Liu, J., Ge, Z., Wang, X. and Cheng X., CFD analysis of transverse flow in a wire-wrapped hexagonal seven-pin bundle, Nuclear Engineering and Design, Vol. 317 (2017), pp. 146-157.

[7] Wang, X. and Cheng, X., Analysis of inter-channel sweeping flow in wire wrapped 19-rod bundle, Nuclear Engineering and Design, Vol. 333 (2018), pp. 115-121.

[8] Hata, K., Takeuchi, Y., Hama, K., Shiotsu, M. and Shirai Y. and Fukuda K., Natural convection heat transfer from a vertical cylinder in liquid sodium, *Mechanical Engineering Journal*, Vol. 1, No. 1 (2014), pp. 1-12.

[9] Hata, K., Fukuda, K. and Mizuuchi, T., "Natural Convection Heat Transfer from Vertical Rod Bundles in Liquid Sodium," *Mechanical Engineering Journal*, Vol. 3, No. 3, pp. 1-16, 2016.

[10] Hata, K., Fukuda, K. and Mizuuchi, T., "Natural Convection Heat Transfer from Vertical 5×5 Rod Bundles in Liquid Sodium," *Journal of Heat Transfer,* Trans. ASME, Vol. 139, pp. 032502-1-11, 2017.

[11] Hata, K., Fukuda, K. and Mizuuchi, T., "Natural Convection Heat Transfer from Vertical 7×7 Rod Bundles in Liquid Sodium," Proceedings of the 25th International Conference on Nuclear Engineering, July 2-6, 2017, Shanghai Convention Center, Shanghai, China, Paper No. ICONE25-66180, pp. 1-13, 2017.

[12] Hata, K., Takeuchi, Y., Shiotsu, M. and Sakurai A., Natural convection heat transfer from a horizontal cylinder in liquid sodium (Part 1: Experimental results), Nuclear Engineering and Design, Vol. 193 (1999), pp. 105-118.

[13] Hata, K., Takeuchi, Y., Shiotsu, M. and Sakurai A., Natural convection heat transfer from a horizontal cylinder in liquid sodium (Part 2: Generalized correlation for laminar natural convection heat transfer), Nuclear Engineering and Design, Vol.194 (1999), pp. 185-196.

[14] Hata, K., Takeuchi, Y., Hama, K. and Shiotsu M., Natural convection heat transfer from horizontal Rod bundles in liquid sodium Part 1: Correlations for two parallel horizontal cylinders based on experimental and theoretical results, Journal of Nuclear Science and Technology, Vol. 52, No.2 (2015), pp. 214-227.

[15] Hata, K., Takeuchi, Y., Hama, K. and Shiotsu M., "Natural convection heat transfer from horizontal Rod bundles in liquid sodium Part 2: Correlations for horizontal rod bundles based on theoretical results," Journal of Nuclear Science and Technology, DOI:10.1080/00223131.2014. 947347, Vol. 52, No.3 (2015), pp. 342-354.

[16] SolidWorks 2011-2012 Education Edition Media Kit, (2011): SolidWorks Japan K.K., Tokyo, (in Japanese).

[17] Spalding D. B., The PHOENICS Beginner's Guide, CHAM Ltd., London, United Kingdom.

[18] Patankar S. V., (1980): *Numerical Heat Transfer and Fluid Flow* (1991), Hemisphere Pub. Corp., New York.

[19] Favre-Marinet, M. and Tardu, S., Convective Heat Transfer (2009), ISTE Ltd and John Wiley & Sons, Inc., Great Britain and United States.

[20] Hanjalic, K., Kenjeres, S., Tummers, M. J.,and Jonker, H. J. J., Analysis and Modeling of Physical Transport Phenomena (2009), Published by VSSD.

[21] LeFevre, E. J. and Ede, A. J., Laminar Free Convection from the Outer Surface of a Vertical Circular Cylinder, Proceedings of the 9th International Congress on Applied Mechanics Brussels, Vol. 4 (1957), pp.175-183.

[22] Mabuchi, I., "Laminar Free Convection from a Vertical Cylinder with Uniform Surface Heat Flux," Trans. Jpn. Soc. Mech. Eng., Vol. 27, No. 180 (1961), pp. 1306-1313 (in Japanese).

[23] Burmeister, L. C., Convective Heat Transfer (1983), John Willy & Sons, p. 536.

6. Conclusions

Nomenclature

Acknowledgments

References

Figure and Table Captions

Table 1 Parameters for calculation.

Fig. 1 Schematic diagram of a test vessel with a 7.6-mm diameter heated cylinder with helical wire spacer.

Fig. 2 Geometry: Vertical single cylinder with helical wire spacer.

Figs. 3 Coordinates for a 7.6-mm diameter heated cylinder with helical wire spacer (d=1.2 mm, gap=0.2 mm and pitch=165 mm): r-θ plane (a), r-z plane (b) and r-θ top plane (c).

Fig. 4 Liquid temperatures in the conductive sub-layer, δ_{CSL}, based on numerically predicted data points (solution of unsteady laminar three dimensional basic equations) for vertical single cylinder with D=7.6 mm.

Fig. 5 Experimental data of local surface temperature rises, $(T_s)_z$-T_L, for vertical single heated cylinder without helical wire spacer versus the vertical distance from the leading edge of the heated section, z, at heat fluxes of 2×10^5 to 2×10^6 W/m^2 compared with the numerical solutions and Eq. (14).

Fig. 6 Heat transfer process on the vertical cylinder of D=7.62 mm and L=186 mm without helical wire spacer compared with heat transfer curves numerically analyzed by δ_{CSL}=200 μm, and thickness of conductive sub-layer, δ_{CSL}.

Fig. 7 Local surface temperature rises, $\{(T_s)_{\theta,z}\}_{w\text{-}s}$-$T_L$, for a vertical single cylinder with helical wire spacer (d=1.2 mm, gap=0.2 mm and pitch=165 mm) versus the vertical distance from the leading edge of the heated section, z, at various peripheral angles (θ=5° to 175°) and heat fluxes.

Fig. 8 Local surface temperature rises, $\{(T_s)_{\theta,z}\}_{w\text{-}s}$-$T_L$, for a vertical single cylinder with helical wire spacer (d=1.2 mm, gap=0.2 mm and pitch=165 mm) versus the vertical distance from the leading edge of the heated section, z, at various peripheral angles (θ=185° to 355°) and heat fluxes.

Fig. 9 Contours of liquid temperature of the r-z plane on θ=105° (a) and the r-θ plane on z=25, 99 and 199 mm from the leading edge of the heated section (b) for a vertical single cylinder with helical wire spacer (d=1.2 mm, gap=0.2 mm and pitch=165 mm) at q =1×10^6 W/m^2.

Fig. 10 The $(v_\theta)_{w\text{-}s}$, $(v_r)_{w\text{-}s}$ and $(v_z)_{w\text{-}s}$, for a vertical single cylinder with helical wire spacer (d=1.2 mm, gap=0.2 mm and pitch=165 mm) on r=3.8 mm versus the vertical distance from the leading edge of the heated section, z, at various peripheral angles (θ=45°, 135°, 225° and 315°) with q =1×10^6 W/m^2.

Fig. 11 Local Nusselt number, $(Nu_{\theta,z})_{w\text{-}s}$, for a vertical single cylinder with helical wire spacer (d=1.2 mm, gap=0.2 mm and pitch=165 mm) versus the vertical distance from the leading edge of the heated section, z, at various peripheral angles (θ=5° to 175°) and heat fluxes.

Fig. 12 Local Nusselt number, $(Nu_{\theta,z})_{w\text{-}s}$, for a vertical single cylinder with helical wire spacer (d=1.2 mm, gap=0.2 mm and pitch=165 mm) versus the vertical distance from the leading edge of the heated section, z, at various peripheral angles (θ=185° to 355°) and heat fluxes.

Fig. 13 Theoretical solutions of $(Nu_{av})_{w\text{-}s}$ for a vertical single cylinder with helical wire spacer (d=1.2 mm, gap=0.2 mm and pitch=165 mm) with authors' correlation, Eq. (31), and Nu_{av} for vertical single cylinder without helical wire spacer with authors' correlation, Eq. (19).

Fig. 14 Comparison of theoretical solutions of $(Nu_{av})_{w\text{-}s}$ for a vertical single cylinder with helical wire spacer (d=1.2 mm, gap=0.2 mm and pitch=165 mm) and Nu_{av} for a vertical single cylinder without helical wire spacer with authors' correlation, Eq. (19).

Fig. 15 Local surface temperature rises, $\{(T_s)_{\theta,z}\}_{w\text{-}s}$-$T_L$, for a vertical single cylinder with helical wire spacer (d=1.2 mm, gap=0.6 mm and pitch=165 mm) versus the vertical distance from the leading edge of the heated section, z, at various peripheral angles (θ=5° to 175°).

Fig. 16 Local surface temperature rises, $\{(T_s)_{\theta,z}\}_{w\text{-}s}$-$T_L$, for a vertical single cylinder with helical wire spacer (d=1.2 mm, gap=0.6 mm and pitch=165 mm) versus the vertical distance from the leading edge of the heated section, z, at various peripheral angles (θ=185° to 355°).

Fig. 17 Local Nusselt number, $(Nu_{\theta,z})_{w\text{-}s}$, for a vertical single cylinder with helical wire spacer (d=1.2 mm, gap=0.6 mm and pitch=165 mm) versus the vertical distance from the leading edge of the heated section, z, at various peripheral angles (θ=5° to 175°).

Fig. 18 Local Nusselt number, $(Nu_{\theta,z})_{w\text{-}s}$, for a vertical single cylinder with helical wire spacer (d=1.2 mm, gap=0.6 mm and pitch=165 mm) versus the vertical distance from the leading edge of the heated section, z, at various peripheral angles (θ=185° to 355°).

Fig. 19 Average Nusselt number, $(Nu_{av})_{w\text{-}s}$, for a vertical single cylinder with helical wire spacer (d=1.2 mm and pitch=165 mm) versus gap at $(Ra_{f,L})_{w\text{-}s}=3.248\times10^6$ (q =1×10^6 W/m^2).

Fig. 20 Comparison of theoretical solutions of $(Nu_{av})_{w\text{-}s}$ for a vertical single cylinder with helical wire spacer at various gaps (d=1.2 mm, gap=0 to 1 mm and pitch=165 mm) with those of Nu_{av} for a vertical single cylinder without helical wire spacer, with authors' correlations, Eq. (19).

Fig. 21 Local surface temperature rises, $\{(T_s)_{\theta,z}\}_{w\text{-}s}$-$T_L$, for a vertical single cylinder with helical wire spacer (d=1.2 mm, gap=0.2 mm and pitch=100 mm) versus the vertical distance from the leading edge of the heated section, z, at various peripheral angles (θ=5° to 175°).

Fig. 22 Local surface temperature rises, $\{(T_s)_{\theta,z}\}_{w\text{-}s}$-$T_L$, for a vertical single cylinder with helical wire spacer (d=1.2 mm, gap=0.2 mm and pitch=100 mm) versus the vertical distance from the leading edge of the heated section, z, at various peripheral angles (θ=185° to 355°).

Fig. 23 Local Nusselt number, $(Nu_{\theta,z})_{w\text{-}s}$, for a vertical single cylinder with helical wire spacer (d=1.2 mm, gap=0.2 mm and pitch=100 mm) versus the vertical distance from the leading edge of the heated section, z, at various peripheral angles (θ=5° to 175°).

Fig. 24 Local Nusselt number, $(Nu_{\theta,z})_{w\text{-}s}$, for a vertical single cylinder with helical wire spacer (d=1.2 mm, gap=0.2 mm and pitch=100 mm) versus the vertical distance from the leading edge of the heated section, z, at various peripheral angles (θ=185° to 355°).

Fig. 25 Average Nusselt number, $(Nu_{av})_{w\text{-}s}$, for a vertical single cylinder with helical wire spacer (d=1.2 mm and gap=0.2 mm) versus pitch at $(Ra_{f,L})_{w\text{-}s}$=3.248×10^6 (q =1×10^6 W/m^2).

Fig. 26 Comparison of theoretical solutions of $(Nu_{av})_{w\text{-}s}$ for a vertical single cylinder with helical wire spacer at various pitches (d=1.2 mm, gap=0.2 mm and pitch=100 to 200 mm) with those of Nu_{av} for a vertical single cylinder without helical wire spacer, with authors' correlations, Eq. (19).

Fig. 27 Local surface temperature rises, $\{(T_s)_{\theta,z}\}_{w\text{-}s}$-$T_L$, for a vertical single cylinder with helical wire spacer (d=1.6 mm, gap=0.2 mm and pitch=165 mm) versus the vertical distance from the leading edge of the heated section, z, at various peripheral angles (θ=5° to 175°).

Fig. 28 Local surface temperature rises, $\{(T_s)_{\theta,z}\}_{w\text{-}s}$-$T_L$, for a vertical single cylinder with helical wire spacer (d=1.6 mm, gap=0.2 mm and pitch=165 mm) versus the vertical distance from the leading edge of the heated section, z, at various peripheral angles (θ=185° to 355°).

Fig. 29 Local Nusselt number, $(Nu_{\theta,z})_{w\text{-}s}$, for a vertical single cylinder with helical wire spacer (d=1.6 mm, gap=0.2 mm and pitch=165 mm) versus the vertical distance from the leading edge of the heated section, z, at various peripheral angles (θ=5° to 175°).

Fig. 30 Local Nusselt number, $(Nu_{\theta,z})_{w\text{-}s}$, for a vertical single cylinder with helical wire spacer (d=1.6 mm, gap=0.2 mm and pitch=185 mm) versus the vertical distance from the leading edge of the heated section, z, at various peripheral angles (θ=185° to 355°).

Fig. 31 Average Nusselt number, $(Nu_{av})_{w\text{-}s}$, for a vertical single cylinder with helical wire spacer (gap=0.2 mm and pitch=165 mm) versus d at $(Ra_{f,L})_{w\text{-}s}=3.248\times10^6$ (q =1×10^6 W/m^2).

Fig. 32 Comparison of theoretical solutions of $(Nu_{av})_{w\text{-}s}$ for a vertical single cylinder with helical wire spacer at various wire diameters (d=1 to 2 mm, gap=0.2 mm and pitch=165 mm) with those of Nu_{av} for a vertical single cylinder without helical wire spacer, with authors' correlations, Eq. (19).

Table 1 Parameters for calculation.

System Pressure (P) [kPa]	101.3								
Cylinder Diameter (D) [mm]	7.6								
Heated Length (L) [mm]	200								
Liquid Temperature (T_L) [K]	673								
Heat Flux (q) [W/m^2]	1×10^4	2×10^4	7×10^4	1×10^5	2×10^5	7×10^5	1×10^6	2×10^6	7×10^6
$(Gr_L^*)_{w\text{-}s}$	5.771×10^9	1.157×10^{10}	4.088×10^{10}	5.877×10^{10}	1.195×10^{11}	4.502×10^{11}	6.698×10^{11}	1.514×10^{12}	8.585×10^{12}
$(Ra_L^*)_{w\text{-}s}$ $\{=(Gr_L^*)_{w\text{-}s}Pr_{w\text{-}s}\}$	2.876×10^7	5.761×10^7	2.029×10^8	2.912×10^8	5.889×10^8	2.168×10^9	3.187×10^9	6.953×10^9	3.533×10^{10}
$(Ra_{f,L})_{w\text{-}s}$ $\{=(Gr_L^*)_{w\text{-}s}Pr_{w\text{-}s}^2/(4+9Pr_{w\text{-}s}^{1/2}+10Pr_{w\text{-}s})\}$	3.059×10^4	6.123×10^4	2.150×10^5	3.081×10^5	6.200×10^5	2.235×10^6	3.248×10^6	6.860×10^6	3.147×10^7
First Control Volume Width for r-component (Δr) [mm]	0.4								
Thickness of the conductive sub-layer (δ_{CSL}) [μm]	200								
Geometry	a vertical single cylinder with helical wire spacer								
Helical wire spacer	Solid with smooth-wall friction								
gap [mm]	0	0.05	0.1	0.2	0.4	0.6	0.8	1	
pitch [mm]	100	160	200						
diameter (d) [mm]	1	1.2	1.6	2					
Coordinate system	Cylindrical coordinates (θ, r, z)								
Control volume	Cut-cell algorithm								
Control volume number	(36, 34, 128)								
Physical model	Laminar model								

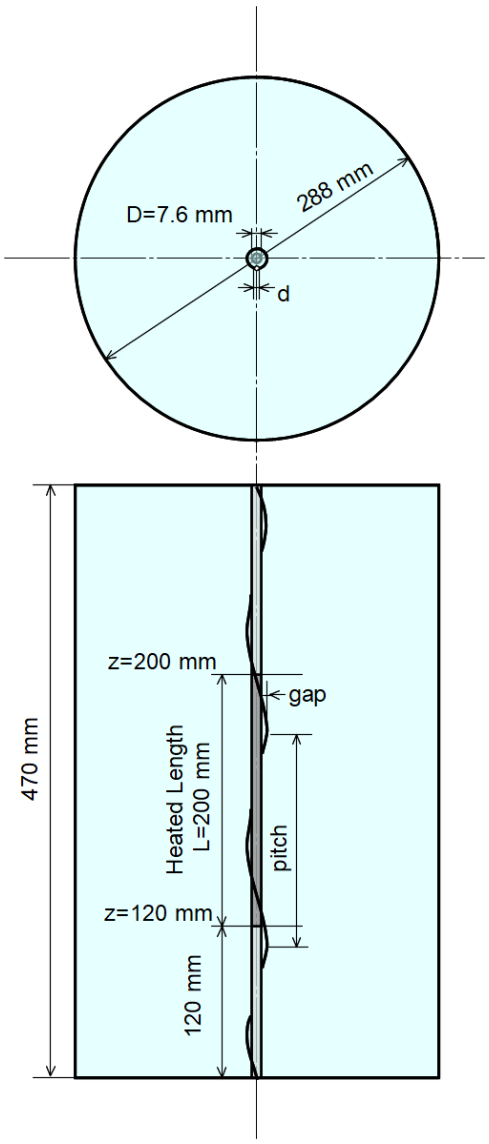

Fig. 1 Schematic diagram of a test vessel with a 7.6-mm diameter heated cylinder with helical wire spacer.

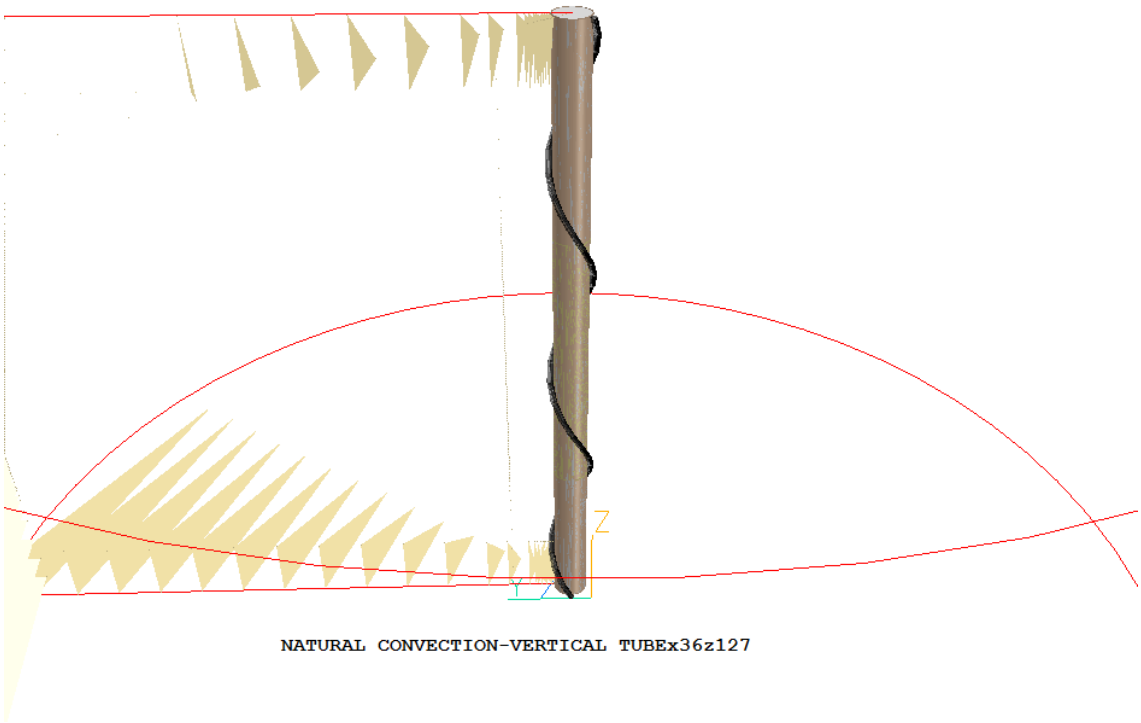

Fig. 2 Geometry: Vertical single cylinder with helical wire spacer.

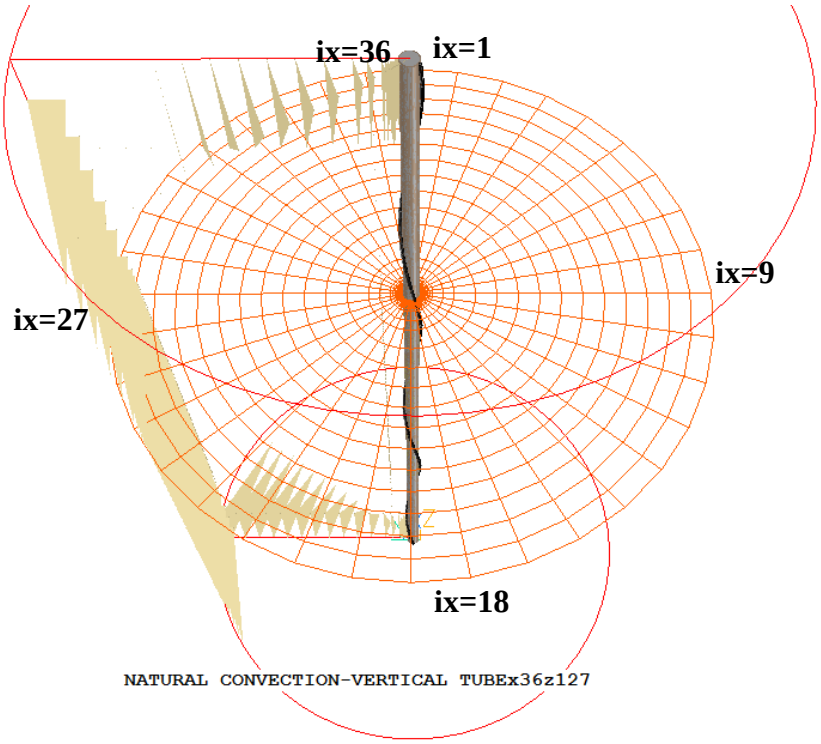
ix=36
ix=1
ix=9
ix=27
ix=18
NATURAL CONVECTION-VERTICAL TUBEx36z127

(a)

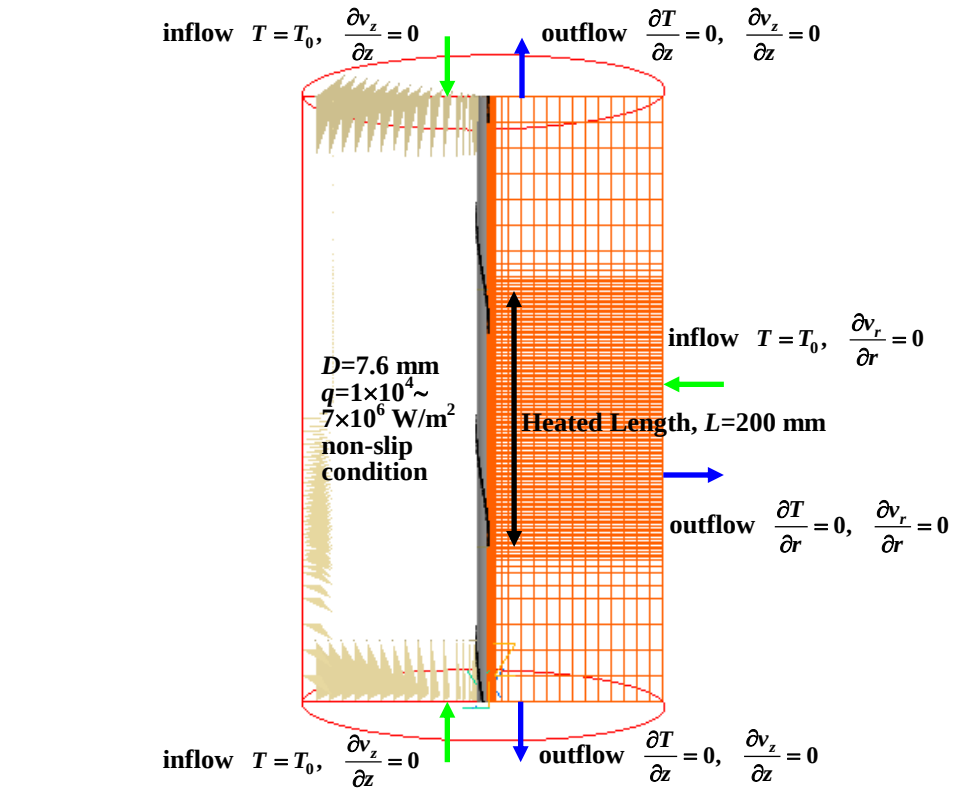
inflow $T = T_0$, $\frac{\partial v_z}{\partial z} = 0$
outflow $\frac{\partial T}{\partial z} = 0$, $\frac{\partial v_z}{\partial z} = 0$
inflow $T = T_0$, $\frac{\partial v_r}{\partial r} = 0$
D=7.6 mm
q=1×10^4~
7×10^6 W/m^2
non-slip
condition
Heated Length, L=200 mm
outflow $\frac{\partial T}{\partial r} = 0$, $\frac{\partial v_r}{\partial r} = 0$
inflow $T = T_0$, $\frac{\partial v_z}{\partial z} = 0$
outflow $\frac{\partial T}{\partial z} = 0$, $\frac{\partial v_z}{\partial z} = 0$
NATURAL CONVECTION-VERTICAL TUBEx36z127

(b)

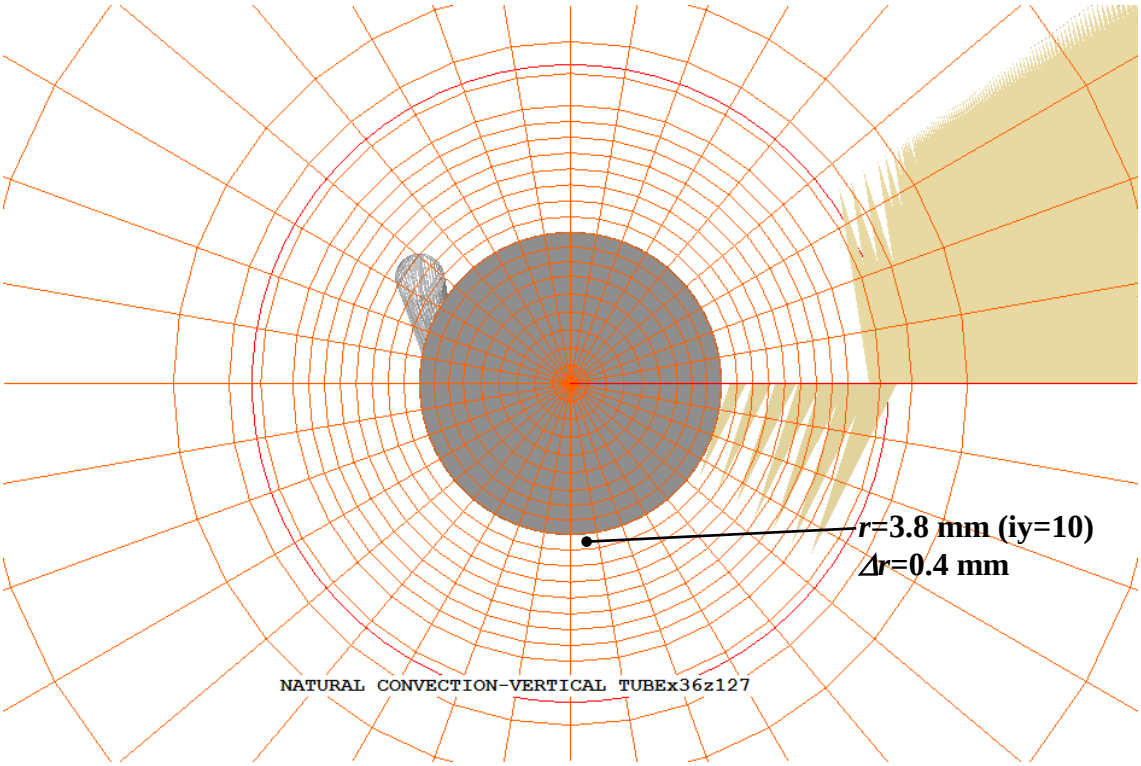

(c)

Figs. 3 Coordinates for a 7.6-mm diameter heated cylinder with helical wire spacer (d=1.2 mm, gap=0.2 mm and pitch=165 mm): r-θ plane (a), r-z plane (b) and r-θ top plane (c).

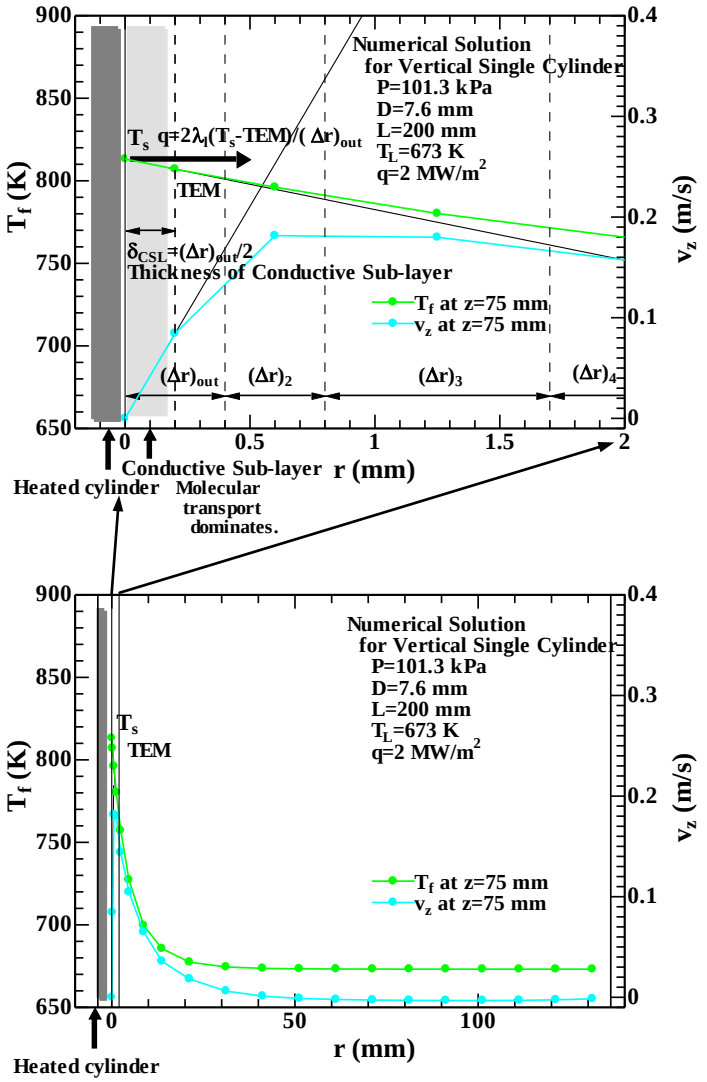

Fig. 4 Liquid temperatures in the conductive sub-layer, δ_{CSL}, based on numerically predicted data points (solution of unsteady laminar three dimensional basic equations) for vertical single cylinder with D=7.6 mm.

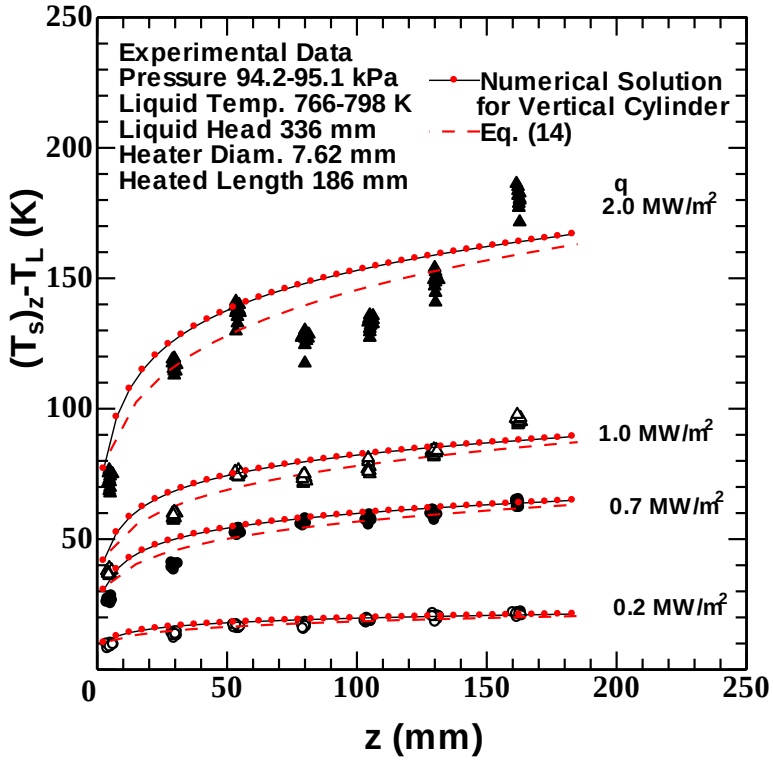

Fig. 5 Experimental data of local surface temperature rises, $(T_s)_z$-T_L, for vertical single heated cylinder without helical wire spacer versus the vertical distance from the leading edge of the heated section, z, at heat fluxes of 2×10^5 to 2×10^6 W/m^2 compared with the numerical solutions and Eq. (14).

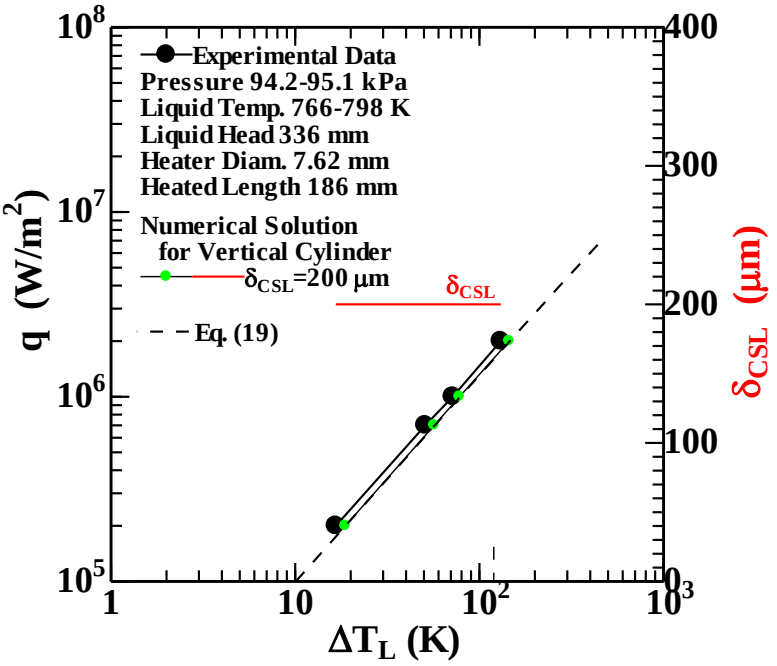

Fig. 6 Heat transfer process on the vertical cylinder of D=7.62 mm and L=186 mm without helical wire spacer compared with heat transfer curves numerically analyzed by δ_{CSL}=200 μm, and thickness of conductive sub-layer, δ_{CSL}.

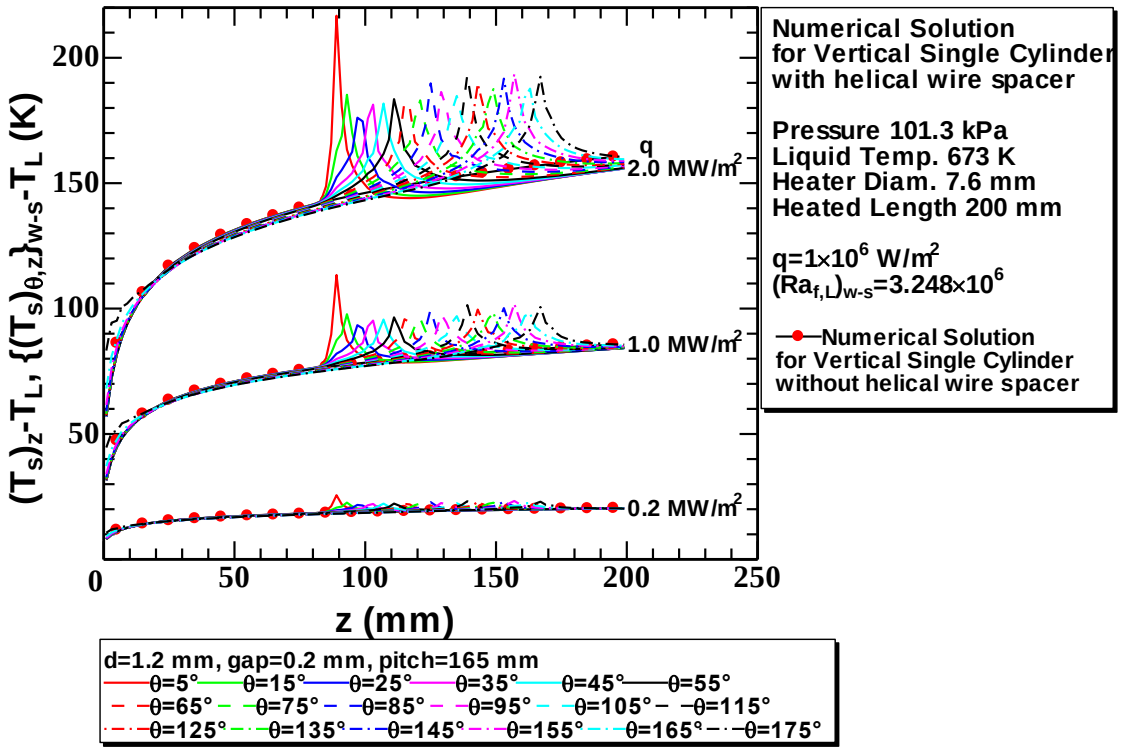

Fig. 7 Local surface temperature rises, $\{(T_s)_{\theta,z}\}_{w\text{-}s}\text{-}T_L$, for a vertical single cylinder with helical wire spacer (d=1.2 mm, gap=0.2 mm and pitch=165 mm) versus the vertical distance from the leading edge of the heated section, z, at various peripheral angles (θ=5° to 175°) and heat fluxes.

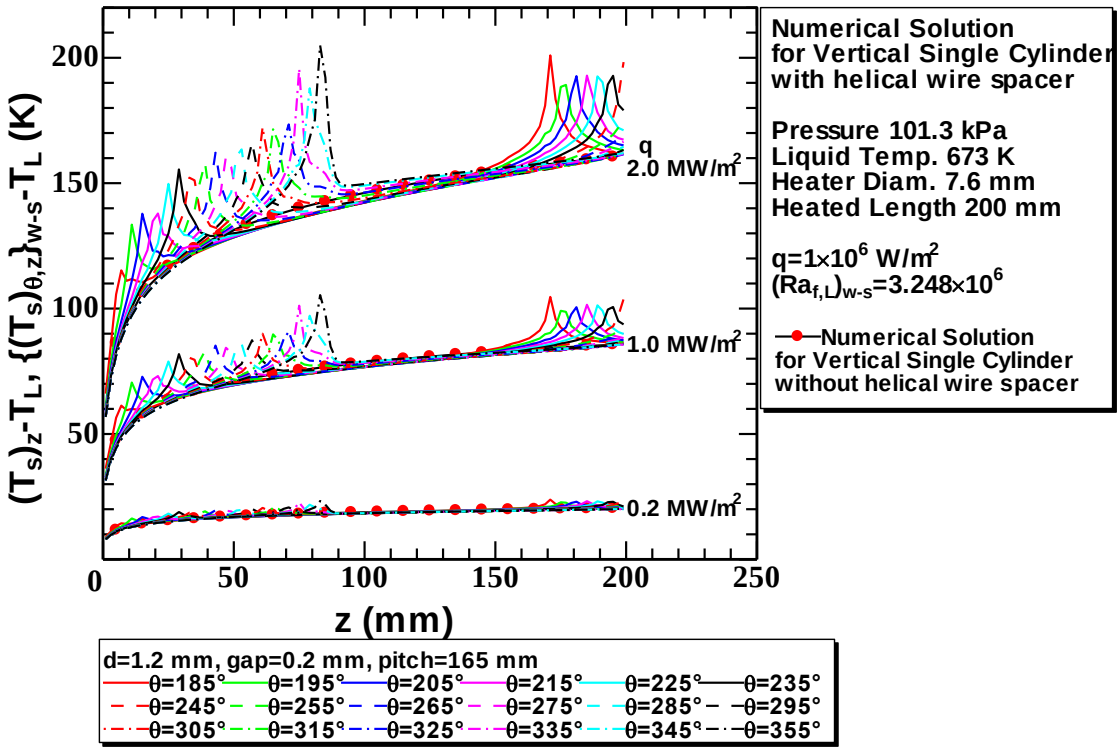

Fig. 8 Local surface temperature rises, $\{(T_s)_{\theta,z}\}_{w\text{-}s}\text{-}T_L$, for a vertical single cylinder with helical wire spacer (d=1.2 mm, gap=0.2 mm and pitch=165 mm) versus the vertical distance from the leading edge of the heated section, z, at various peripheral angles (θ=185° to 355°) and heat fluxes.

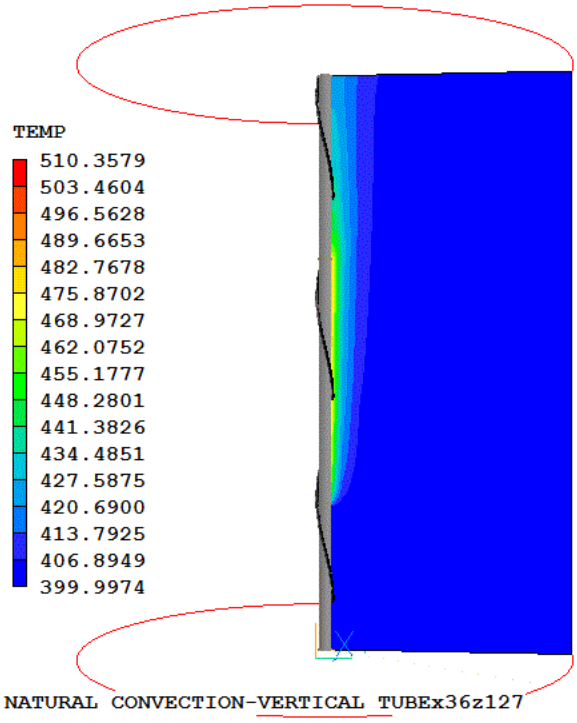
TEMP
510.3579
503.4604
496.5628
489.6653
482.7678
475.8702
468.9727
462.0752
455.1777
448.2801
441.3826
434.4851
427.5875
420.6900
413.7925
406.8949
399.9974
NATURAL CONVECTION-VERTICAL TUBEx36z127

(a)

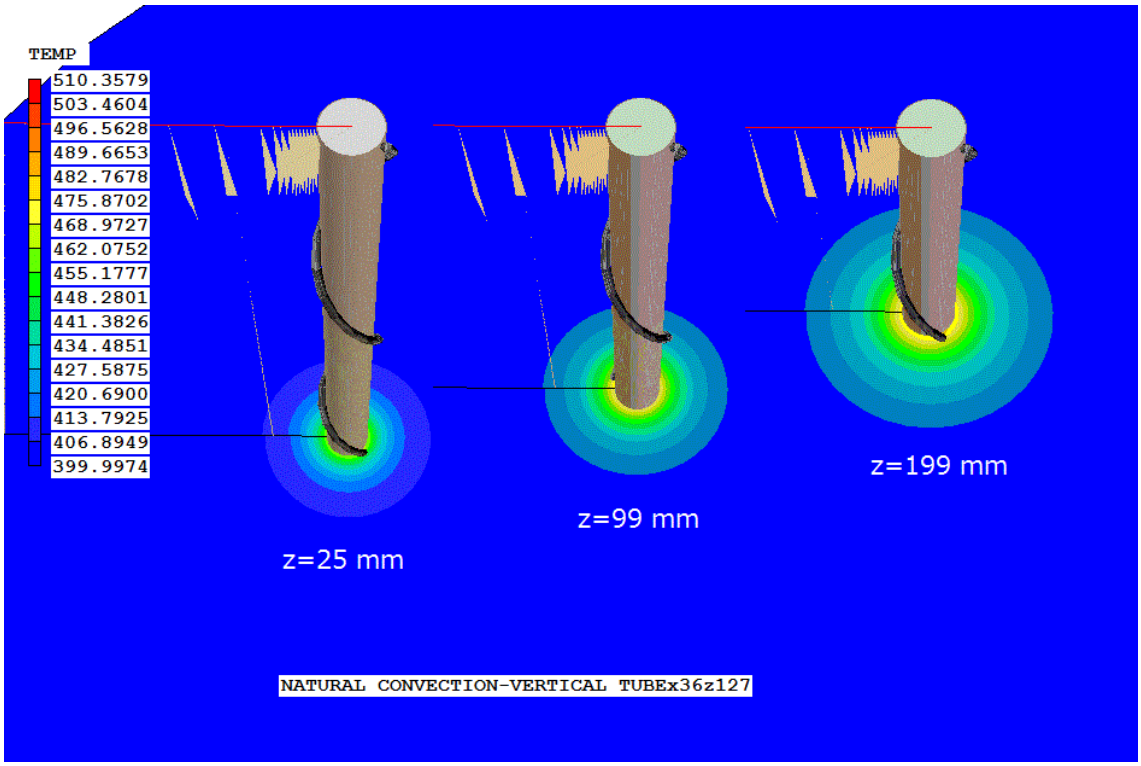

(b)

Fig. 9 Contours of liquid temperature of the *r*-*z* plane on θ=105° (a) and the *r*-θ plane on *z*=25, 99 and 199 mm from the leading edge of the heated section (b) for a vertical single cylinder with helical wire spacer (*d*=1.2 mm, gap=0.2 mm and pitch=165 mm) at $q = 1\times10^6$ W/m^2.

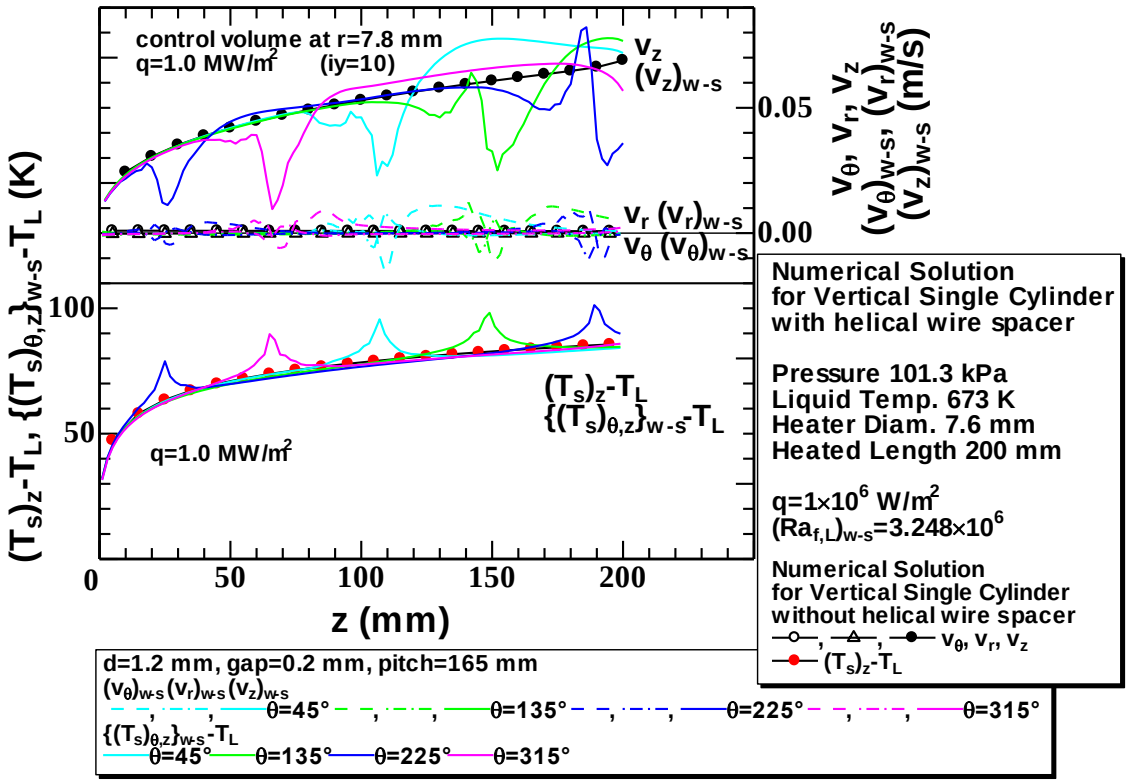

Fig. 10 The $(v_\theta)_{w\text{-}s}$, $(v_r)_{w\text{-}s}$ and $(v_z)_{w\text{-}s}$, for a vertical single cylinder with helical wire spacer (d=1.2 mm, gap=0.2 mm and pitch=165 mm) on r=3.8 mm versus the vertical distance from the leading edge of the heated section, z, at various peripheral angles (θ=45°, 135°, 225° and 315°) with q =1×10^6 W/m^2.

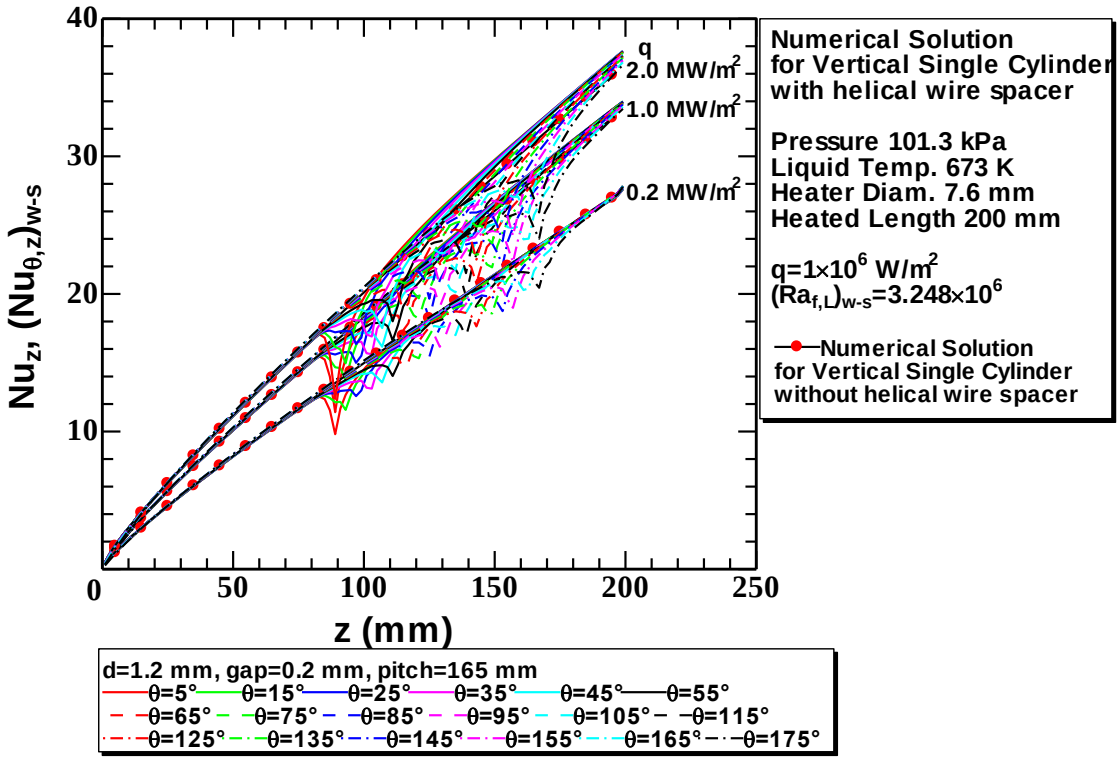

Fig. 11 Local Nusselt number, $(Nu_{\theta,z})_{w\text{-}s}$, for a vertical single cylinder with helical wire spacer (d=1.2 mm, gap=0.2 mm and pitch=165 mm) versus the vertical distance from the leading edge of the heated section, z, at various peripheral angles (θ=5° to 175°) and heat fluxes.

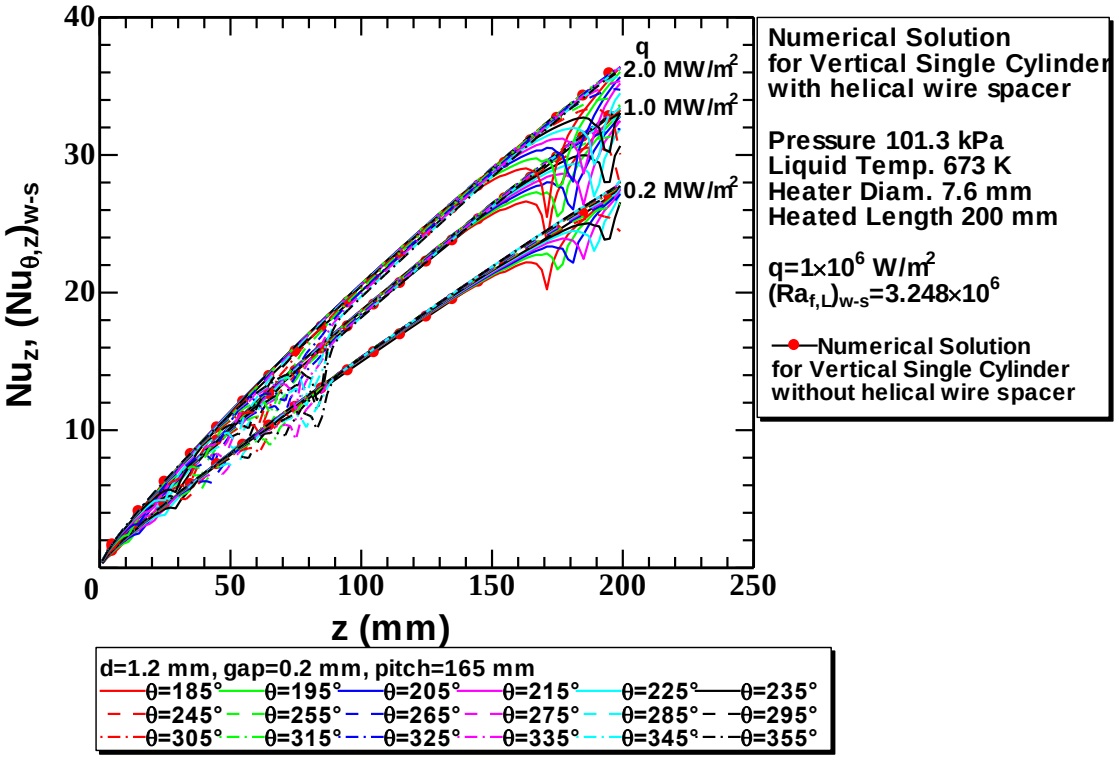

Fig. 12 Local Nusselt number, $(Nu_{\theta,z})_{w\text{-}s}$, for a vertical single cylinder with helical wire spacer (d=1.2 mm, gap=0.2 mm and pitch=165 mm) versus the vertical distance from the leading edge of the heated section, z, at various peripheral angles (θ=185° to 355°) and heat fluxes.

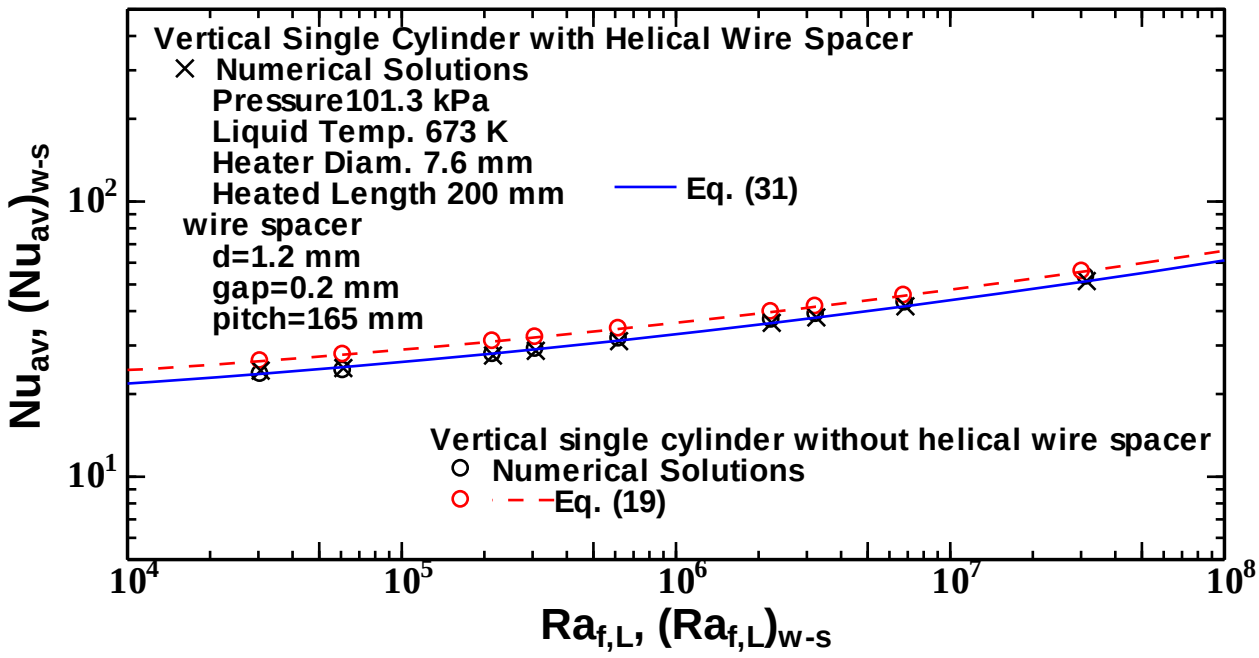

Fig. 13 Theoretical solutions of $(Nu_{av})_{w\text{-}s}$ for a vertical single cylinder with helical wire spacer (d=1.2 mm, gap=0.2 mm and pitch=165 mm) with authors' correlation, Eq. (31), and Nu_{av} for vertical single cylinder without helical wire spacer with authors' correlation, Eq. (19).

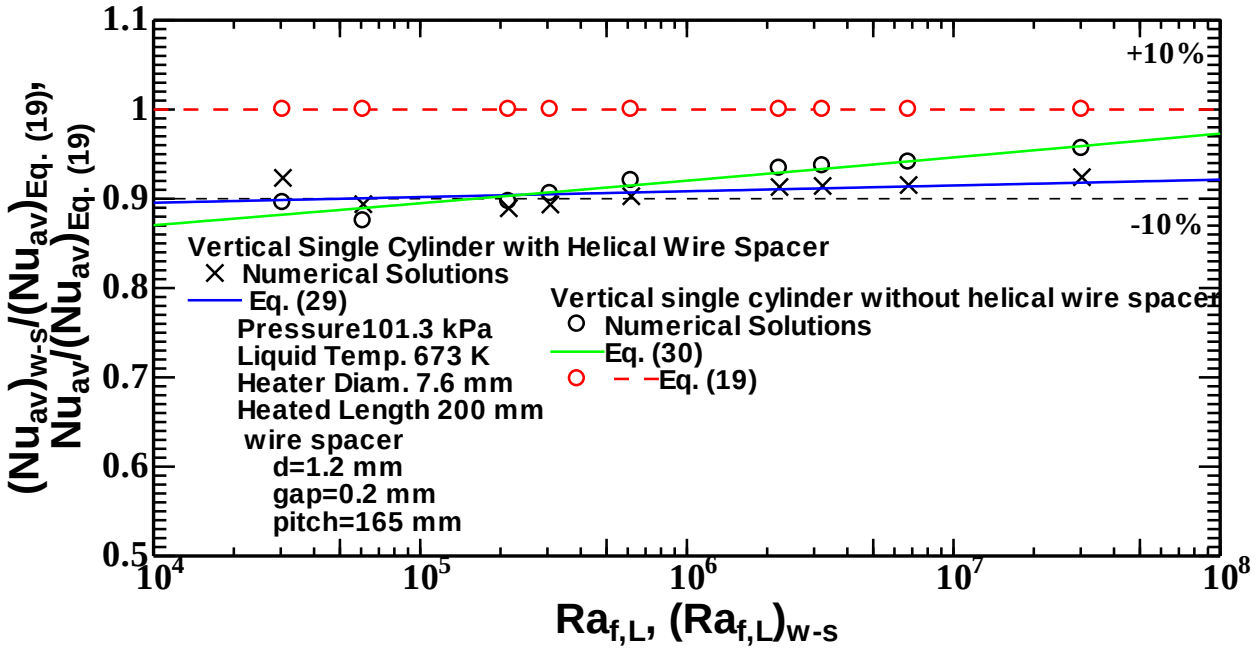

Fig. 14 Comparison of theoretical solutions of $(Nu_{av})_{w\text{-}s}$ for a vertical single cylinder with helical wire spacer (d=1.2 mm, gap=0.2 mm and pitch=165 mm) and Nu_{av} for a vertical single cylinder without helical wire spacer with authors' correlation, Eq. (19).

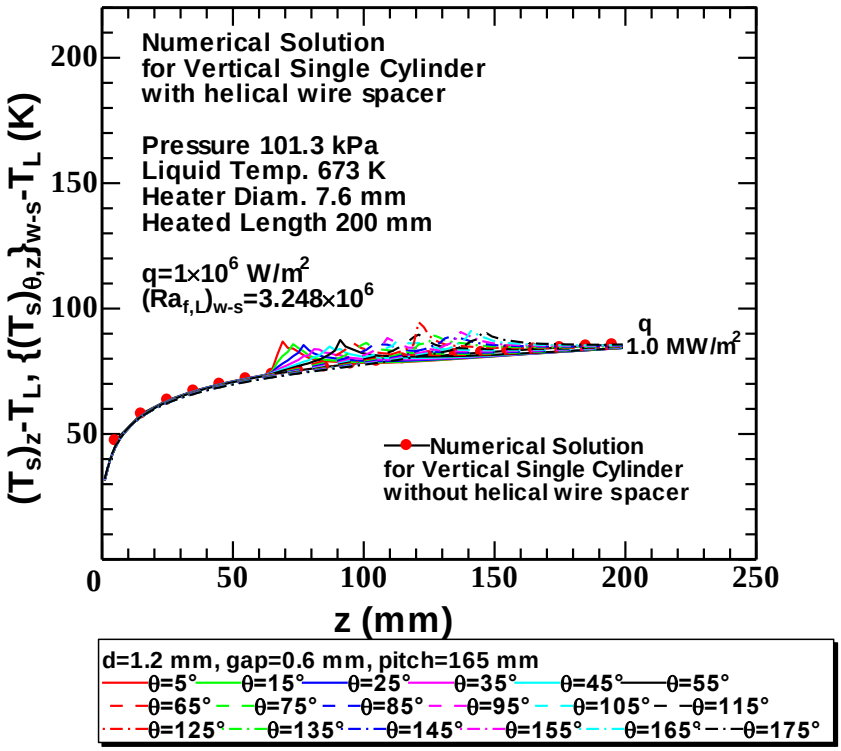

Fig. 15 Local surface temperature rises, $\{(T_s)_{\theta,z}\}_{w\text{-}s}$-$T_L$, for a vertical single cylinder with helical wire spacer (d=1.2 mm, gap=0.6 mm and pitch=165 mm) versus the vertical distance from the leading edge of the heated section, z, at various peripheral angles (θ=5° to 175°).

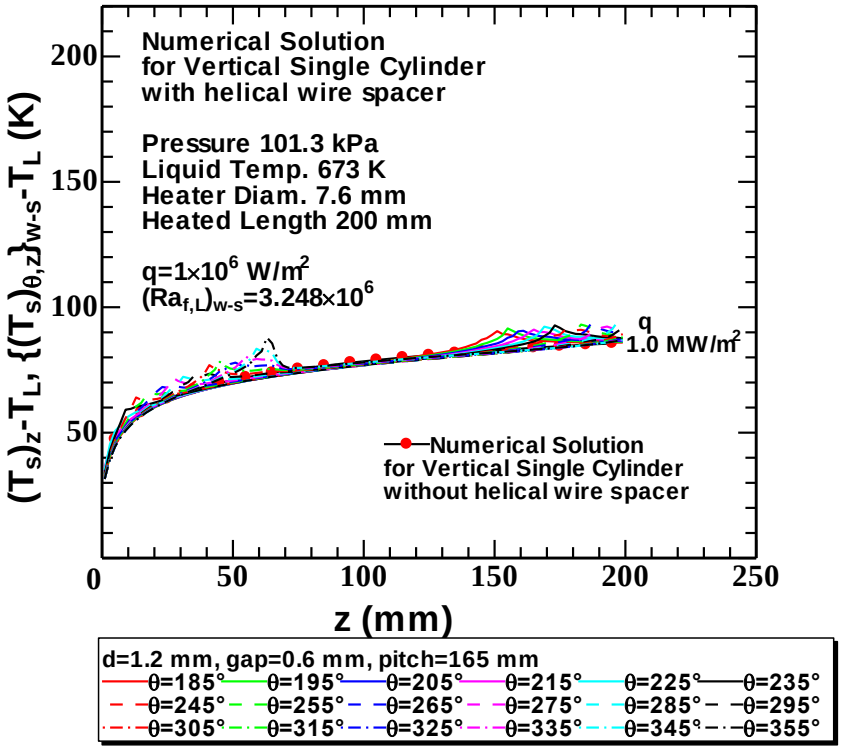

Fig. 16 Local surface temperature rises, $\{(T_s)_{\theta,z}\}_{w\text{-}s}\text{-}T_L$, for a vertical single cylinder with helical wire spacer (d=1.2 mm, gap=0.6 mm and pitch=165 mm) versus the vertical distance from the leading edge of the heated section, z, at various peripheral angles (θ=185° to 355°).

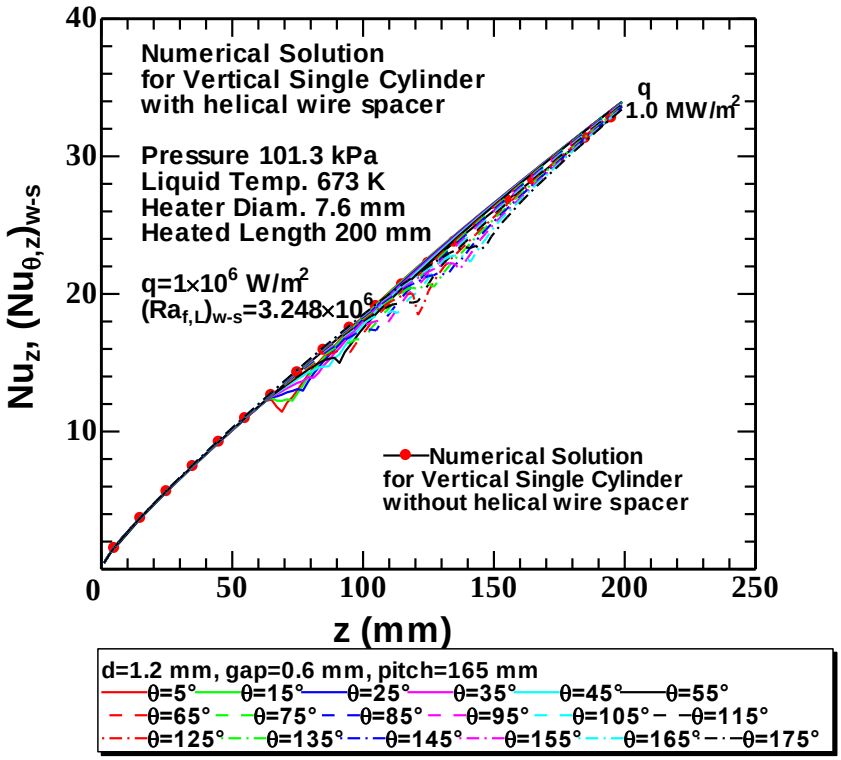

Fig. 17 Local Nusselt number, $(Nu_{\theta,z})_{w\text{-}s}$, for a vertical single cylinder with helical wire spacer (d=1.2 mm, gap=0.6 mm and pitch=165 mm) versus the vertical distance from the leading edge of the heated section, z, at various peripheral angles (θ=5° to 175°).

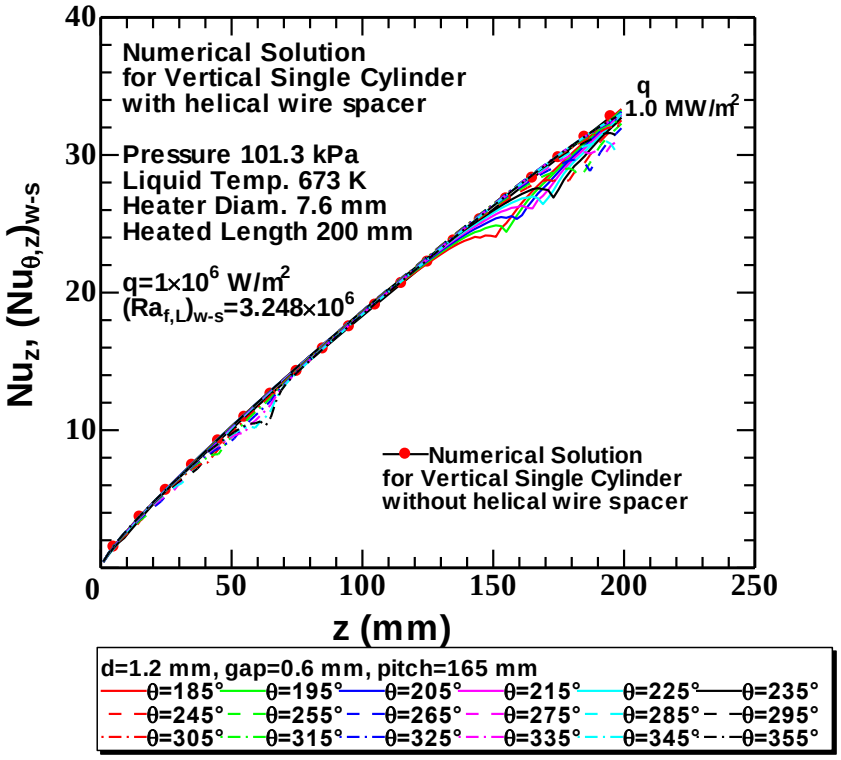

Fig. 18 Local Nusselt number, $(Nu_{\theta,z})_{w\text{-}s}$, for a vertical single cylinder with helical wire spacer (d=1.2 mm, gap=0.6 mm and pitch=165 mm) versus the vertical distance from the leading edge of the heated section, z, at various peripheral angles (θ=185° to 355°).

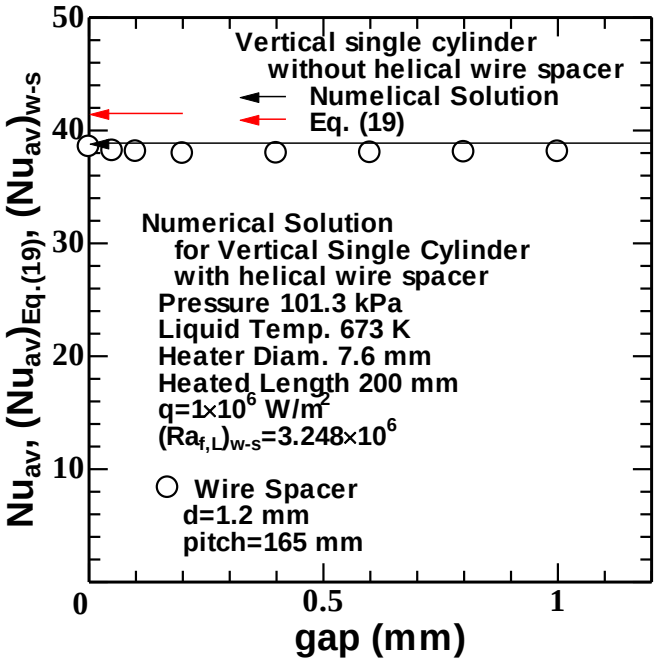

Fig. 19 Average Nusselt number, $(Nu_{av})_{w\text{-}s}$, for a vertical single cylinder with helical wire spacer (d=1.2 mm and pitch=165 mm) versus gap at $(Ra_{f,L})_{w\text{-}s}=3.248\times10^6$ (q =1×10^6 W/m^2).

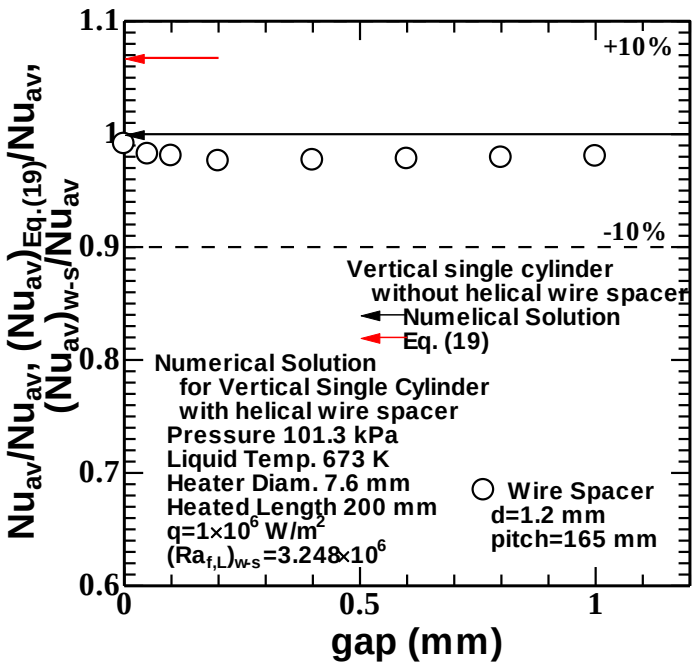

Fig. 20 Comparison of theoretical solutions of $(Nu_{av})_{w\text{-}s}$ for a vertical single cylinder with helical wire spacer at various gaps (d=1.2 mm, gap=0 to 1 mm and pitch=165 mm) with those of Nu_{av} for a vertical single cylinder without helical wire spacer, with authors' correlation, Eq. (19).

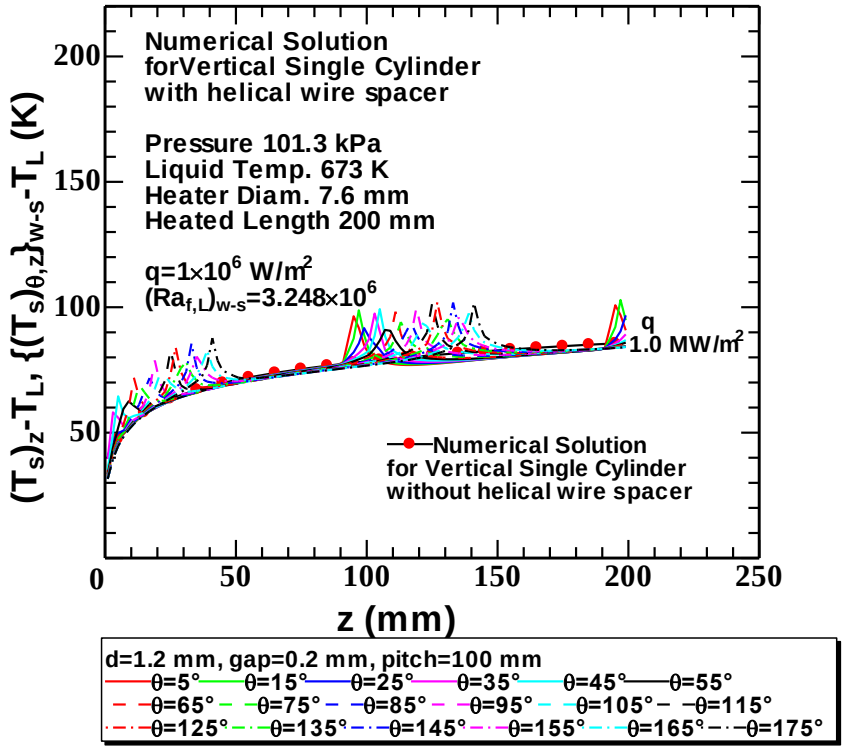

Fig. 21 Local surface temperature rises, $\{(T_s)_{\theta,z}\}_{w\text{-}s}\text{-}T_L$, for a vertical single cylinder with helical wire spacer (d=1.2 mm, gap=0.2 mm and pitch=100 mm) versus the vertical distance from the leading edge of the heated section, z, at various peripheral angles (θ=5° to 175°).

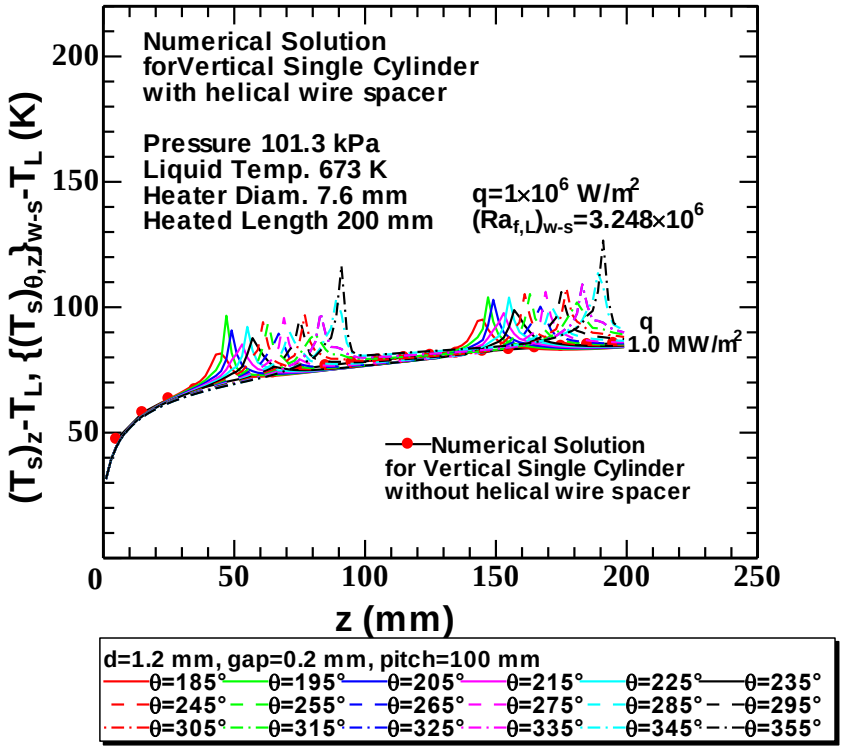

Fig. 22 Local surface temperature rises, $\{(T_s)_{\theta,z}\}_{w\text{-}s}$-$T_L$, for a vertical single cylinder with helical wire spacer (d=1.2 mm, gap=0.2 mm and pitch=100 mm) versus the vertical distance from the leading edge of the heated section, z, at various peripheral angles (θ=185° to 355°).

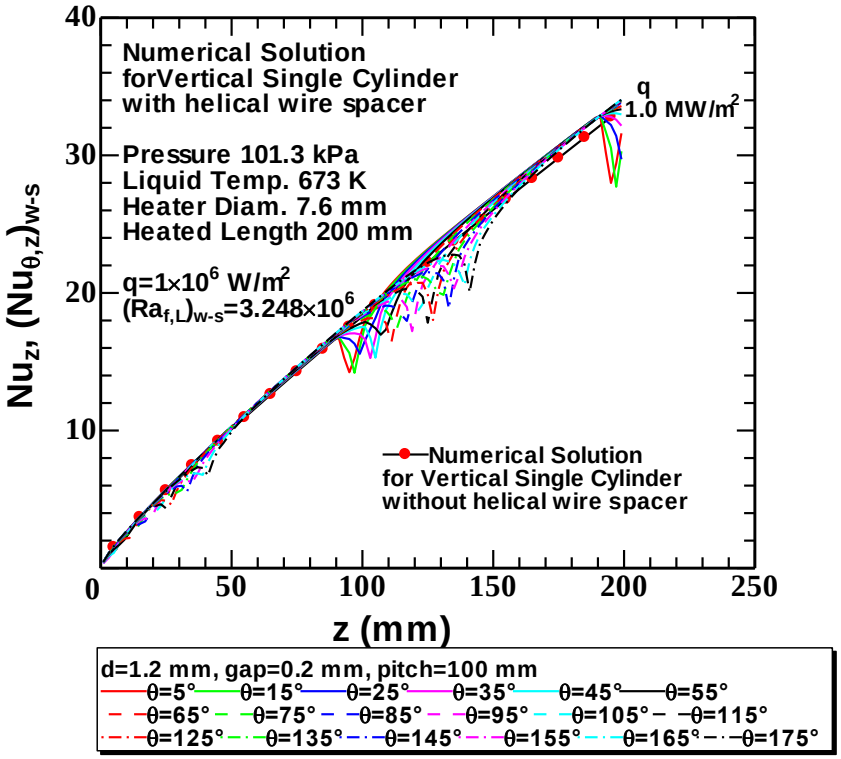

Fig. 23 Local Nusselt number, $(Nu_{\theta,z})_{w\text{-}s}$, for a vertical single cylinder with helical wire spacer (d=1.2 mm, gap=0.2 mm and pitch=100 mm) versus the vertical distance from the leading edge of the heated section, z, at various peripheral angles (θ=5° to 175°).

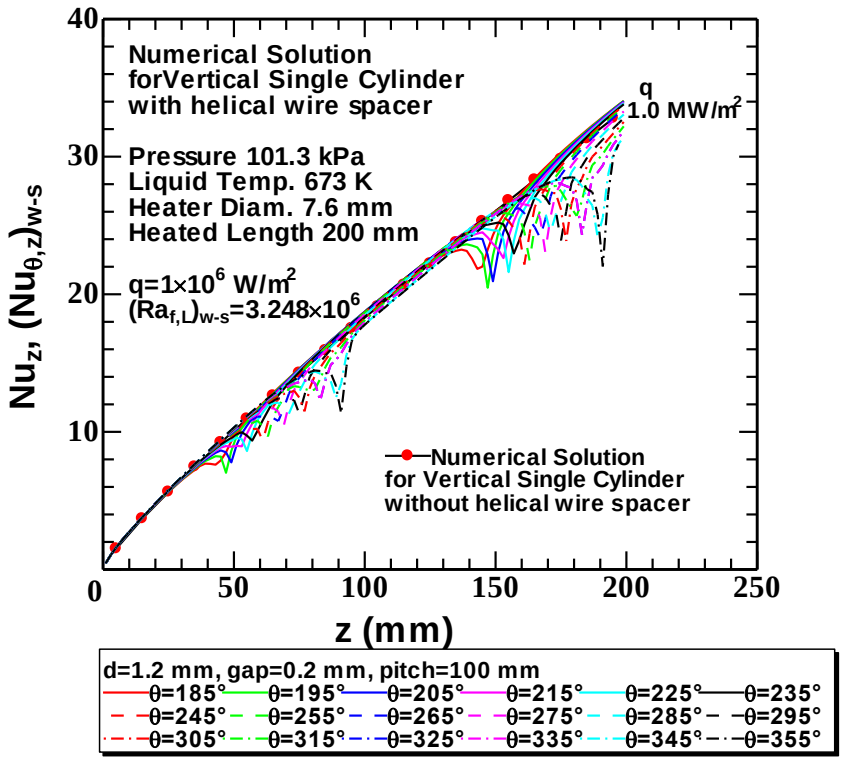

Fig. 24 Local Nusselt number, $(Nu_{\theta,z})_{w\text{-}s}$, for a vertical single cylinder with helical wire spacer (d=1.2 mm, gap=0.2 mm and pitch=100 mm) versus the vertical distance from the leading edge of the heated section, z, at various peripheral angles (θ=185° to 355°).

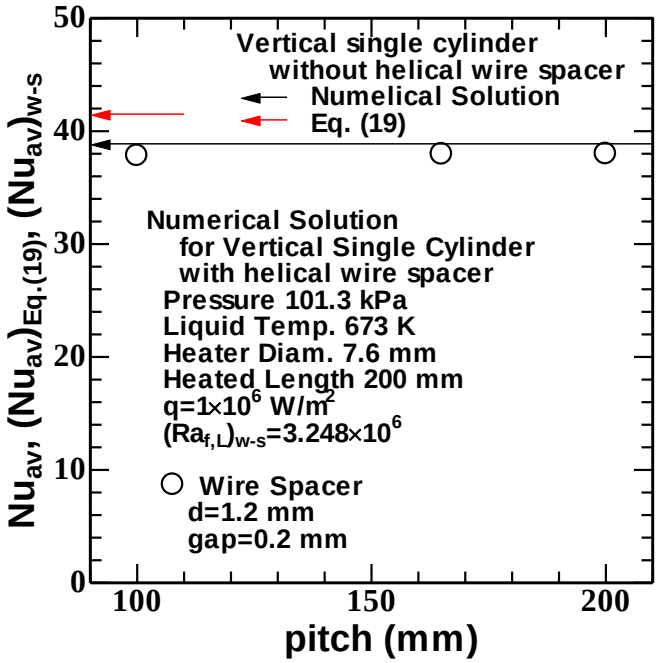

Fig. 25 Average Nusselt number, $(Nu_{av})_{w\text{-}s}$, for a vertical single cylinder with helical wire spacer (d=1.2 mm and gap=0.2 mm) versus pitch at $(Ra_{f,L})_{w\text{-}s}=3.248\times10^6$ (q =1×10^6 W/m^2).

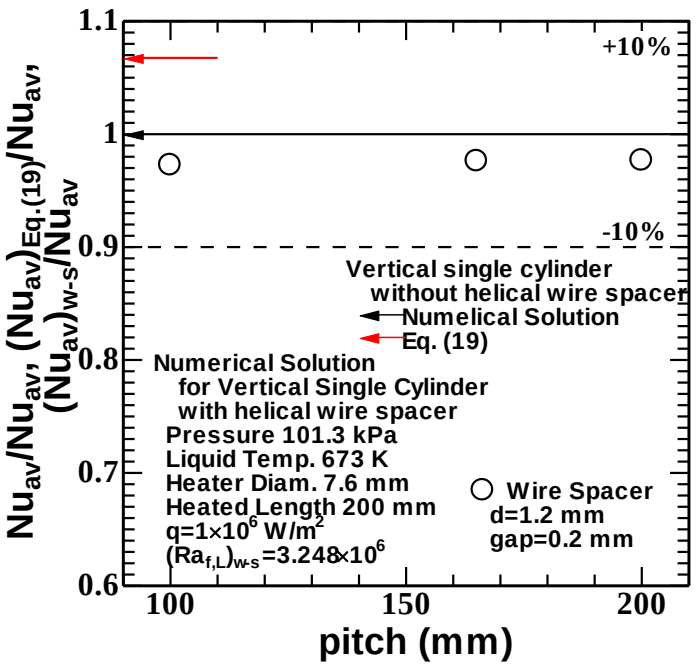

Fig. 26 Comparison of theoretical solutions of $(Nu_{av})_{w\text{-}s}$ for a vertical single cylinder with helical wire spacer at various pitches (d=1.2 mm, gap=0.2 mm and pitch=100 to 200 mm) with those of Nu_{av} for a vertical single cylinder without helical wire spacer, with authors' correlation, Eq. (19).

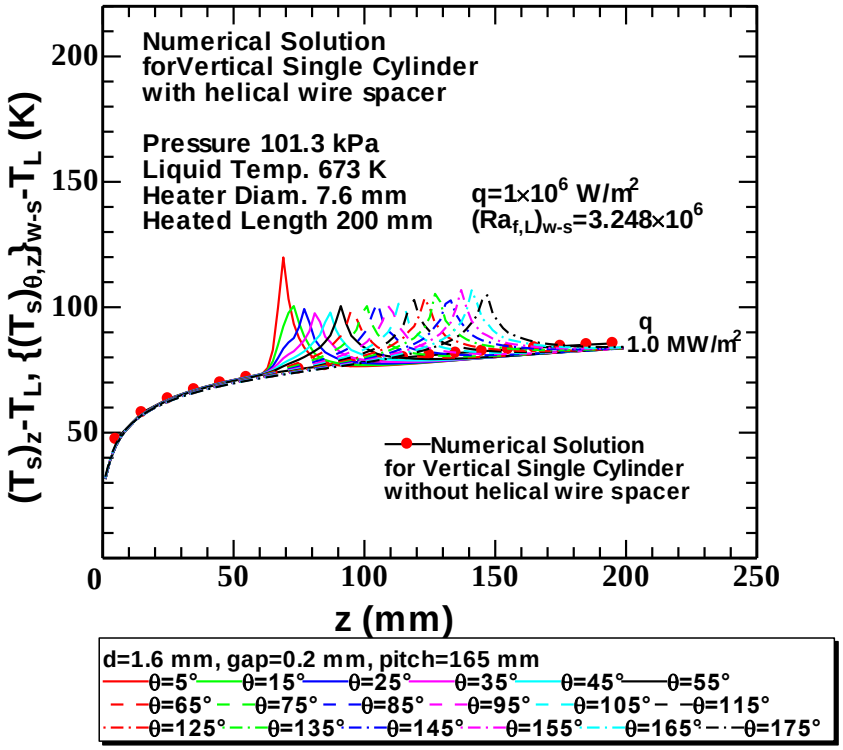

Fig. 27 Local surface temperature rises, $\{(T_s)_{\theta,z}\}_{w\text{-}s}$-$T_L$, for a vertical single cylinder with helical wire spacer (d=1.6 mm, gap=0.2 mm and pitch=165 mm) versus the vertical distance from the leading edge of the heated section, z, at various peripheral angles (θ=5° to 175°).

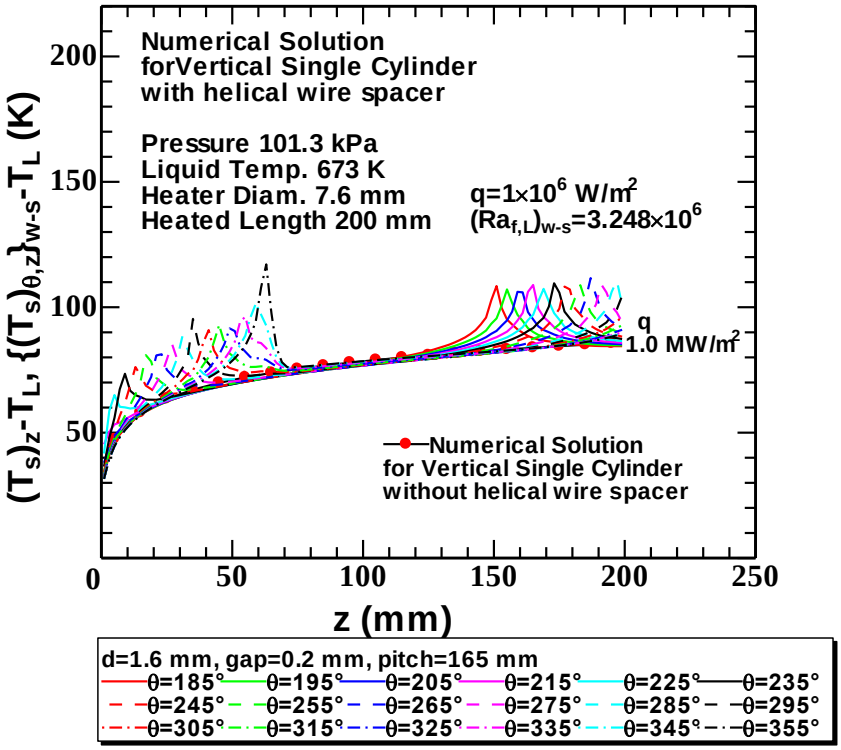

Fig. 28 Local surface temperature rises, $\{(T_s)_{\theta,z}\}_{w\text{-}s}\text{-}T_L$, for a vertical single cylinder with helical wire spacer (d=1.6 mm, gap=0.2 mm and pitch=165 mm) versus the vertical distance from the leading edge of the heated section, z, at various peripheral angles (θ=185° to 355°).

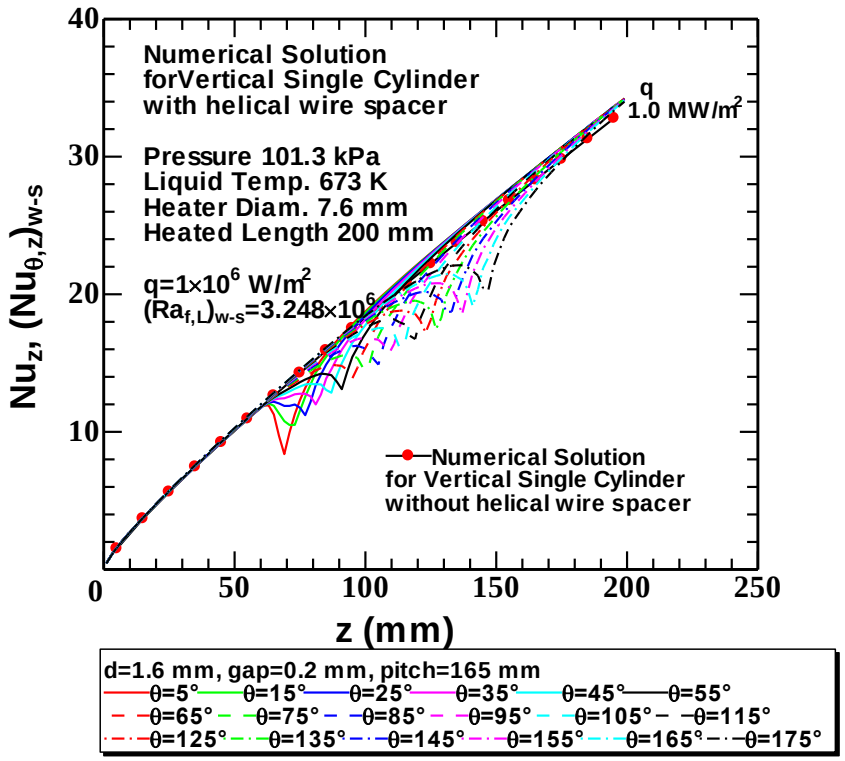

Fig. 29 Local Nusselt number, $(Nu_{\theta,z})_{w\text{-}s}$, for a vertical single cylinder with helical wire spacer (d=1.6 mm, gap=0.2 mm and pitch=165 mm) versus the vertical distance from the leading edge of the heated section, z, at various peripheral angles (θ=5° to 175°).

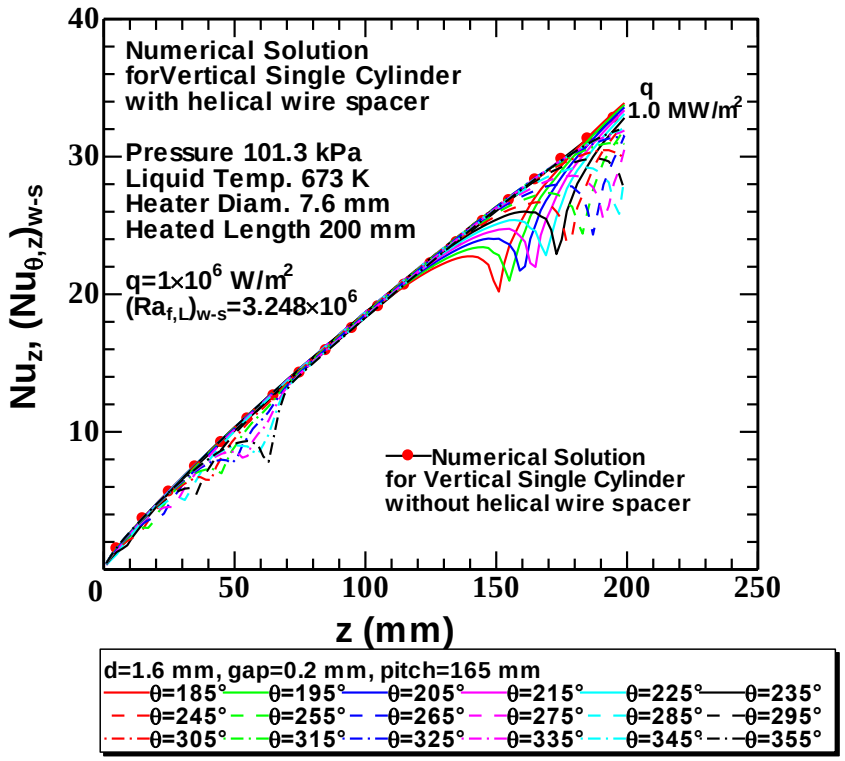

Fig. 30 Local Nusselt number, $(Nu_{\theta,z})_{w\text{-}s}$, for a vertical single cylinder with helical wire spacer (d=1.6 mm, gap=0.2 mm and pitch=185 mm) versus the vertical distance from the leading edge of the heated section, z, at various peripheral angles (θ=185° to 355°).

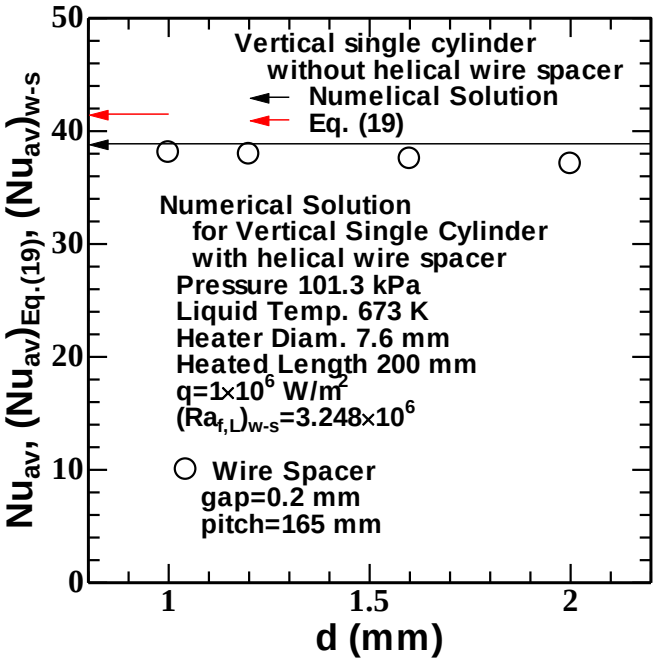

Fig. 31 Average Nusselt number, $(Nu_{av})_{w\text{-}s}$, for a vertical single cylinder with helical wire spacer (gap=0.2 mm and pitch=165 mm) versus d at $(Ra_{f,L})_{w\text{-}s}=3.248\times10^6$ (q =1×10^6 W/m^2).

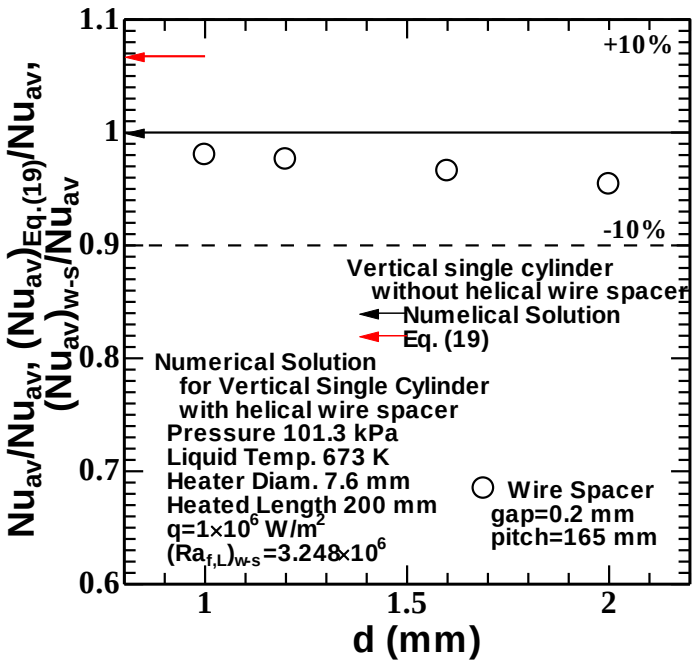

Fig. 32 Comparison of theoretical solutions of $(Nu_{av})_{w\text{-}s}$ for a vertical single cylinder with helical wire spacer at various wire diameters (d=1 to 2 mm, gap=0.2 mm and pitch=165 mm) with those of Nu_{av} for a vertical single cylinder without helical wire spacer, with authors' correlation, Eq. (19).